Acute temporal, regional, and cell-type specific NKCC1 disruption following severe TBI in the developing gyrencephalic brain

Authors:
Alexandra Hochstetler[1,2], Ya'el Courtney[2,3], Peace Oloko[1], Benjamin Baskin[1], Andrew Ding-Su [1], Tawny Stinson[1], Declan McGuone[4], Robin Haynes[2], Maria K. Lehtinen[2,3], and Beth Costine-Bartell[1]*
*Corresponding Author, bcostinebartell@mgh.harvard.edu

Affiliations:
[1]Department of Neurosurgery, Massachusetts General Hospital, Harvard Medical School, Boston, MA 02115
[2]Department of Pathology, Boston Children's Hospital and Harvard Medical School, Boston, MA 02115
[3]Graduate Program in Neuroscience, Harvard Medical School, Boston, MA 02115
[4]Department of Pathology, Yale University School of Medicine, New Haven, CT, 06510

Conflict of Interest statement:
The authors declare no competing financial interests.

Acknowledgements:
This work is supported by NIH NICHD K01HD083759 and R01 HD099397 (BCB), by the Pappendick Family Translational Research Program (MKL), the Hydrocephalus Association, and R01 HD090064 (RH). AH was supported by T32NS007473 and F32NS134588 training fellowships from the National Institute for Neurological Disorders and Stroke. YC was supported by the Howard Hughes Medical Institute through the James J. Gilliam Fellowships for Advanced Study program. PO was supported by a Mass General Summer Research Trainee Program (SRTP). We thank the Boston Children's Hospital IDDRC Cellular Imaging Core supported by S10OD016453. We thank the past and present team of undergraduate interns in the Costine-Bartell laboratory who assisted with the surgeries and 30 hours of intensive care to create the brain injury model and tissue collection as well as the Knight Surgical Research Lab for assistance with anesthesia to create the brain injuries. We are especially grateful for the fetal piglet tissue obtained from Dr. Ryann Fame (Stanford University Department of Neurosurgery), Dr. Mercedes Paredes (University of California, San Francisco (UCSF) Department of Neurology), and Dr. Misty Williams-Fritze (CBSET) and postnatal piglet tissue obtained from Dr. Corinna Beale (Center for Comparative Medicine, MGH). We thank Dr. Cameron Sadegh (UC Davis Department of Neurosurgery) and members of the Lehtinen Laboratory for assistance with prenatal swine brain dissections. We are deeply grateful to participating families for their courage and generosity in consenting to the use of their children in research. We also thank the clinicians, medical examiners, and pathologists who helped in the accrual of cases, including Drs. Gary Dale, Jeffrey Goldstein, Steven Campman, Catherine Stoos, and Colin Smith. We thank Elisabeth Haas and Richard Goldstein for the processing and analysis of infant cases. We thank Jane's Trust Initiative, the NIH NeuroBioBank, and the Edinburgh Brain Bank.

Author contributions:
AH: Conceptualization, investigation, methodology, formal analysis, writing-original draft, visualization; YC: Investigation, methodology, formal analysis, writing-original draft**;** PO: Investigation, methodology, formal analysis, visualization**;** BB: Investigation, methodology, formal analysis, visualization**;** AD: Investigation, methodology**;** DM: Investigation, formal analysis, writing-revising**;** TS: Investigation, methodology**;** RH: Investigation, methodology, formal analysis, writing-revising, funding acquisition**;** MKL: Writing-revising, funding acquisition**;** BCB: Conceptualization, investigation, methodology, visualization, writing-original draft, project administration, funding acquisition

Abstract: Traumatic brain injury (TBI) in children is a leading cause of morbidity and mortality, with no effective treatment and limited clinical management. We developed a multifactorial traumatic brain injury model in piglets which mirrors the evolving pathophysiology of severe pediatric TBI, showing age-dependent hypoxic-ischemic cerebral cortical injury and matrix metalloproteinase-driven vasogenic edema, with infant piglets experiencing less tissue damage than toddler piglets. Extracellular matrix breakdown can precipitate neuronal dysfunction, disrupting chloride homeostasis and the reversal potential for GABA. We hypothesized that ongoing tissue damage might be related to markers of "immature GABA", evaluated by changes to the expression and phosphorylation of sodium-potassium-2-chloride cotransporter 1 (NKCC1), potassium-chloride cotransporter 2 (KCC2), and a regulatory kinase, (STE20/SPS1-related proline-alanine-rich protein kinase) SPAK. We mapped these markers in developing swine and infant human brain, identifying a postnatal pNKCC1 decrease in human infant hippocampus, and a perinatal cortical and hippocampal GABA switch in pigs, with no change in the thalamus. In infant piglets with severe TBI, upregulation of neuronal pNKCC1 correlated with hypoxic-ischemic injury and seizure duration. We also observed dysregulation of NKCC1, KCC2, and SPAK in cortex and hippocampus in infant and toddler piglets with severe TBI, with thalamus unchanged. We noted ectopic, non-apical localization of pNKCC1 signal in choroid plexus epithelium across ages in piglets and humans with severe TBI, indicating acute dysregulation of the CSF chloride milieu. These findings position swine as a useful model for pediatric TBI research and suggest that SPAK or NKCC1 inhibition in infants may be therapeutic.

Significance statement: Severe TBI in early childhood, the majority of which is due to abuse, remains an understudied area of neurotrauma. Our piglet model effectively replicates the pathophysiology of severe pediatric TBI, capturing age-dependent injury patterns and mechanisms of spreading hypoxic-ischemic injury throughout the cortical ribbon. We identified upregulation of neuronal-pNKCC1 in infant piglets, but not toddler piglets with severe TBI, and found this correlates with injury severity, seizure duration, and subarachnoid hemorrhage. Our findings indicate that treatments targeted to inhibit neuronal NKCC1 might alleviate evolving brain injury in infants with severe TBI. This model provides a valuable platform for studying mechanisms of TBI and testing new interventions, potentially advancing therapeutic strategies for pediatric brain injury where stopping traumatic seizures is difficult.

INTRODUCTION:

In childhood, severe traumatic brain injury (TBI) commonly arises from abusive head trauma (AHT), causing high mortality and persistent neurological comorbidities (Keenan et al., 2003). Children of different ages show distinct structural, biomechanical, and physiological vulnerabilities, influencing both injury severity and long-term outcomes. Animal models which enable scaling of injuries to brain volume can help us better understand and treat TBI in pediatric populations.

Swine models are especially valuable as models of age-dependent traumatic brain injury and neurological comorbidities (Clancy et al., 2007; Lind, 2007; Swindle, 1998; Dobbing and Sands 1979). For example, a standardized focal cortical impact produces a larger contusion in piglets approximating human toddlers than in those approximating human infants. Conversely, younger piglets are more prone to diffuse injuries from non-impact rotational forces, similar to clinical observations (Missios et al., 2009; Ibrahim et al., 2010).

We developed a multifactorial brain injury model in piglets which recapitulates a “hemispheric hypodensity” (HH) pattern akin to that observed in pediatric TBI patients, where infant piglets show bilateral HH and toddler piglets show unilateral patterns (Costine-Bartell et al., 2019; Duhaime and Durham 2007; Foster et al., 2014). We have found that subarachnoid hemorrhage with at least 60 minutes of seizure are key drivers of age-dependent hypoxic-ischemic type injury and vasogenic edema (Costine-Bartell et al., 2021; Hochstetler, Pret al., 2024). Maintaining proper ion homeostasis in the developing brain is crucial for neurodevelopment and may be disrupted in TBI. A critical factor in these age-dependent differences may be the “GABA switch”—the developmental transition of GABAergic signaling from primarily excitatory to inhibitory as the brain matures, governed by an increase in the expression and membrane phosphorylation/activity of KCC2 over NKCC1, chloride cotransporters which control neuronal $[Cl^-]_i$ (Ben-Ari 2014; LoTurco et al., 1995). TBI might disrupt this balance, thereby exacerbating injury and its consequences (Bortone and Polleux, 2009).

Anti-seizure medications (GABA agonists) are the standard of care for children with severe TBI to halt traumatic seizures (Smith et al., 2016). In cases of high extracellular chloride such as in early development or injury, GABA agonists may potentiate neuronal excitability and ongoing tissue damage.

The timing of the developmental “GABA switch” from primarily excitatory to inhibitory varies widely across species, but always depends on the relative abundance and activity of two cation chloride cotransporters, NKCC1 (sodium-potassium-2-chloride cotransporter) and KCC2 (potassium-chloride cotransporter) which work in antagonism to control neuronal $[Cl]_i$. In precocial mammals like sheep and guinea pigs, the shift occurs largely before birth, whereas in altricial mammals such as rabbits and rodents, or hatched species such as birds, turtles, and frogs, the switch takes place predominantly after birth (Ben-Ari et al., 2007; Ben-Ari 2014; Sedmak et al., 2016; Tang et al., 2020; Peerboom and Wierenga, 2021). Humans and non-human primates appear to follow a more perinatal pattern (Khazipov et al., 2001; Sedmak et al., 2016). Swine are considered sometimes precocial, and sometimes semi-altricial, thus, pinpointing when the GABA switch occurs is critical for understanding their suitability as a model for pediatric brain injury and for testing age-appropriate anticonvulsant therapies (Young et al., 2023; Bienboire-Frosini et al., 2023). The timing of the GABA switch is also important when considering other diagnoses where seizure activity may play a role in pathogenesis (ex. Sudden Unexpected Death in Childhood) (Goldstein and Poduri 2024; Leitner et al., 2022; Harowitz et al., 2021; Haynes et al., 2021; Patodia et al., 2021).

In this study, we characterized the developmental expression and phosphorylation of NKCC1 and KCC2 in the neonatal human hippocampus and the developing piglet brain and examined how severe TBI disrupts this balance. We hypothesized that developmental differences in NKCC1 expression may contribute to distinct TBI injury patterns in infant and toddler piglets. To address this hypothesis, we employ spatial transcriptomics, immunohistochemistry, and Western blot analyses across developmental stages, brain regions, and TBI conditions. We also examined human TBI autopsy samples from various ages, assessing pNKCC1 expression in different brain compartments and cell types.

119 **MATERIALS AND METHODS:**

120 **Sample procurement**

121 *Animal procedures*

122 All protocols and procedures performed were in accordance with the guidelines of the American Veterinary
123 Association, the National Institutes of Health, and the United States Department of Agriculture. They were
124 approved by the Institutional Animal Care and Use Committee at Massachusetts General Hospital.

125 *Naïve swine tissue collection*

126 ***Prenatal collections***

127 Preterm piglets were collected from euthanized Yorkshire sows at approximately 30% gestation (ED36), 75%
128 gestation (ED90), and 90% gestation (ED105). Pig fetuses were surgically removed from the amniotic sac
129 following maternal euthanasia, rinsed under cold running water, brains were dissected on ice, and tissues were
130 immediately flash frozen. In all cases, the time from euthanasia to sample collection was less than 4 hours.

131 ***Postnatal collections***

132 7 day old (PND7, "infant") and 30 day old (PND30, "toddler") male Yorkshire piglets were selected for naïve
133 tissue collection. Surgery and anesthesia protocols were employed as previously described (BCB et al., 2019a)
134 adjusted to the age of the piglets. In brief, piglets were sedated with ketamine/xylazine/atropine and anesthetized
135 by 1-1.5% isoflurane with medical oxygen. Piglets were intubated and mechanically ventilated with room air. An
136 ear intravenous (IV), or external jugular vein catheter was placed to access venous blood and deliver saline
137 infusion. In all cases, mean arterial blood pressure, oxygen saturation, heart rate and end tidal CO_2, respiratory
138 rate, and core body temperature were managed for the duration of the procedures. A craniotomy was performed,
139 and the dura was removed. Euthasol was delivered intravenously, and then fresh tissue dissection was
140 performed immediately on wet ice. Samples (n=4/age) were collected from August 2023 to October 2023 and
141 flash-frozen on dry ice.

142 *Pediatric severe TBI swine tissue collection*

143 Samples were requisitioned as freezer aliquots from prior studies but are distinct aliquots from the same piglets
144 published in Hochstetler, Price *et al.* 2024. In brief, a series of PND7 and PND30 male Yorkshire piglets from

145 September 2016 to October 2019 were exposed to surgery and anesthesia protocols as detailed above in
146 "postnatal collections". *Immediately prior to injury*, piglets were switched to a seizure-permissive anesthesia
147 protocol and subjected to a combination of injuries scaled to brain volume as previously described (Costine-
148 Bartell et al., 2019; Costine-Bartell et al., 2021) including cortical impact, mass effect, subdural
149 hematoma/subarachnoid hemorrhage supplemented with kainic acid, one minute of apnea, and 10 minutes of
150 hypoventilation. In the sham piglets, only the burr holes and duration of anesthesia were modeled. Piglets were
151 managed in an intensive care monitoring unit for 24 hours after injury. For fresh frozen tissue, euthasol was
152 delivered intravenously, and then fresh tissue dissection followed immediately on wet ice, and samples were
153 flash-frozen on dry ice. For perfused-fixed tissue, piglets were transcardially perfused with room temperature
154 normal saline at a rate of ~1L/min until complete surface vessel clearing followed by room temperature 10%
155 neutral buffered formalin at the same rate until total body stiffness. Brains were obtained and post-fixed in 10%
156 neutral buffered formalin for 3-5 days until appropriate tissue stiffness was achieved.

157 *Human tissue collection*

158 Lysates from frozen hippocampus at the level of the lateral geniculate nucleus were collected from either the
159 NIH NeuroBioBank or the San Diego County Medical Examiner's office, the latter available for research under
160 the auspice of the California Code, Section 27491.41. All infants died suddenly and unexpectedly with the cause
161 of death determined at autopsy and adjudicated within the laboratory for research purposes (Table 1). Unstained
162 tissue sections from FFPE blocks were procured from autopsy brain samples (TBI or non-TBI control) performed
163 at the Neuropathology Department at the University of Edinburgh. Permission to use the brain tissue was given
164 according to the guidelines required by the respective ethics committees of these institutions: the Boston
165 Children's Hospital and Massachusetts General Hospital Institutional Review Boards. Demographic information
166 of all human samples is detailed in Table 1.

167 **Standard laboratory techniques**

168 *Western Blotting*

169 Fresh frozen samples were manually homogenized in N-PER lysis buffer (ThermoScientific #87792)
170 supplemented with 1X Halt (ThermoScientific #78440) protease and phosphatase inhibitor cocktail and lysed at

171 4°C for 60 minutes with end-over-end agitation. Lysates were spun at 16,000 x g for 10 minutes to pellet debris.
172 Supernatants were aliquoted and Pierce BCA assay was used protein concentration (ThermoScientific #23250).
173 20µg of the sample was reduced with 5X Laemmli Sample Buffer (BioLegend #426311) supplemented with B-
174 mercaptoethanol (5%) and diluted with double distilled water to an equivalent volume. Samples were heated at
175 70°C for 5 minutes, loaded into 4-12% Bis-Tris gels (NuPage #NP0321) and separated at 140V for 65 minutes.
176 Gels were transferred to 0.2 µm nitrocellulose membranes at 1.0A for 30 minutes using the Bio-Rad Trans-
177 Blotter® system. Membranes were stained with Ponceau-S total protein stain blocked with 5% milk dissolved in
178 1X Tris Buffered Saline-0.1% Tween-20 (TBST) with gentle agitation. Membranes were incubated with primary
179 antibody diluted in 5% milk-TBST, washed with TBST, and then incubated with secondary antibody diluted in
180 5% milk-TBST. Membranes were washed with TBST and TBS, exposed with chemiluminescent reagents
181 (Cytiva-Amersham #RPN2235), and visualized on a Bio-Rad Chemi-Doc Imager. For antibody validation, full
182 complete membranes were first probed with each antibody to evaluate non-specific bands, specific bands and
183 dimers, and to optimize dilutions. In the case of pNKCC1 and NKCC1 antibodies, our laboratory has performed
184 in-house knock-down validation. All validation methods are presented in Table 2. For publication gels, technical
185 duplicate membranes were cut at 80kDa to allow probing of 1) pSPAK, 2) SPAK, and 3) beta-actin (below 80kDa)
186 simultaneously with 1) pNKCC1, 2) NKCC1, and 1) pKCC2, 2) KCC2 (above 80kDa). In all cases, band
187 intensities were normalized to total protein loaded (Ponceau stain) for the graphs, since beta-actin and beta-
188 tubulin were found to be poor loading controls across age and region. Membrane stripping was performed with
189 ReStore™ Western Blot Stripping Solution and protocol (ThermoScientific #21059).

190 *Quantitative, Real-Time PCR*

191 Samples were processed for RNA extraction using the Total RNA Miniprep Kit (New England BioLabs #T2010),
192 evaluated for concentration >50ng/µL and a quality ratio of A260/280 of >2.0. RNA was prepared for cDNA
193 synthesis with +reverse transcriptase and –reverse transcriptase reactions using the LunaScript® RT Supermix
194 Kit (New England Biolabs #E3010) using quality control metrics of concentration >100ng/µL and A260/280 ratio
195 >1.8. Samples were diluted to equivalent cDNA loading and probed with Taqman™ reagents for quantitative

196 gene expression using fast run chemistry on an Applied Biosystems machine. In all cases, -RT and no template
197 controls were run for each sample. Probe information is detailed in Table 3.

198 *Spatial Transcriptomics*

199 Spatial transcriptomics was conducted on anatomically matched formalin-fixed, paraffin-embedded (FFPE) brain
200 sections from a sham 30-day-old piglet and a 30-day-old piglet with severe traumatic brain injuries using
201 NanoString GeoMx® Digital Spatial Profiling technology, facilitated by the Comparative Pathology and Genomics
202 Shared Resource core facility at The Cummings School of Veterinary Medicine at Tufts University. Regions of
203 interest (ROIs) were selected to capture key anatomical areas relevant to age-dependent TBI pathology and
204 neuroinflammation. Following ROI selection, samples underwent GeoMx® platform analysis, where regions were
205 scanned, and digital counts were obtained for gene targets of interest. Signal thresholding at a 3% cutoff was
206 applied to exclude low-expression signals, ensuring that only significant transcript data were included in
207 downstream analysis. Normalization was performed using internal controls (External RNA Control Consortium)
208 provided by the GeoMx® platform to account for technical variation across slides and samples. Upper quartile
209 normalization was performed after filtering the dataset to remove targets below the limit of quantitation.

210 *Histology*

211 Following immersion fixation, brains were washed with 1X phosphate-buffered saline (PBS), paraffin embedded
212 and sectioned at 5-μm thickness and mounted onto silanized glass slides. Immunofluorescence was performed
213 on these sections using antibodies detailed in Table 2. Briefly, sections were deparaffinized in xylenes,
214 rehydrated, and then subjected to antigen retrieval in boiling 10mM citric acid-Tween pH 6.0 for 20 minutes.
215 Staining protocols are presented in more detail below. In all cases, negative control sections were incubated in
216 corresponding species-specific IgG at an equivalent concentration to the primary antibody dilution during the
217 primary antibody incubation step. For figures where quantitation is presented, all slides evaluated were stained
218 together in a single batch to minimize signal variability. Slides were imaged on a Zeiss Axio Observer D1 inverted
219 microscope (fluorescent, 20x air objective), an Olympus BX51 light microscope (chromogenic, 10x or 20x air
220 objective), or a Zeiss LSM980 (20x air or 63x oil objective) at the Boston Children's Hospital Cellular Imaging
221 Core. Images were processed and assembled using ZEN Blue, ImageJ software, and Adobe Illustrator.

222 ***Chromogenic Immunohistochemistry***

223 For chromogenic stains, a peroxidase quenching step was performed immediately prior to antigen retrieval.
224 Sections were then permeabilized for 5 minutes with 1% PBS-Tween-20 and blocked for 1 hour using normal
225 horse serum diluted in Super Sensitive Wash Buffer (BioGenex, HK583-5KEGP). Sections were incubated in
226 primary antibodies diluted in blocking buffer for 2 hours at room temperature. Slides were washed with 1% PBS-
227 Tween-20 and then incubated in the secondary antibody diluted in blocking buffer for 30 minutes. Sections were
228 washed and subjected to antibody visualization with Vectastain® ABC and DAB reagents (VectorLabs), counter
229 stained with Mayer's hematoxylin plus bluing reagent, and then dehydrated, cleared, and mounted with resin-
230 based medium (Cytoseal™ 60 Mounting Medium, Epredia).

231 ***Fluorescent Immunohistochemistry***

232 Sections were permeabilized for at least 10 minutes with 0.3% Triton X-100 in PBSand subsequently blocked
233 for at least 40 minutes at room temperature with blocking solution (3% donkey serum and 2% BSA). Following,
234 sections were washed with PBS and incubated in primary antibody diluted in blocking solution for 2 hours at
235 room temperature. Next, sections were washed again and incubated in secondary antibody diluted in blocking
236 solution for 1 hour at room temperature. Sections were washed and exposed to Hoechst 33342 nuclear stain for
237 five minutes and mounted with an aqueous mounting medium (Fluoromount-G™).

238 *Study design*

239 The evaluation of the GABA switch in the naïve swine brain was planned prospectively and the maximum
240 biological replicates were collected as allowed by protocol restrictions. Sample size, demographics, and
241 characteristics are detailed in Figure 1A'. Postnatal samples were analyzed first to determine if the study was
242 sufficiently powered. Following this power analysis, all naïve swine samples were analyzed together to generate
243 heat maps and scatterplots in Figure 1. For the spatial transcriptomics experiment, Figure 3, the region of interest
244 was the experimental unit.

245 The evaluation of frozen human hippocampus was performed in the BCH Department of Pathology. A series of
246 infants who died from non-TBI causes was used. Samples with an extended postmortem interval (PMI) (>30
247 hours) were excluded because prolonged PMI positively correlated with NKCC1 expression, likely a reflection of

248 tissue autolysis in our pilot analysis. The effect of TBI injuries in swine on the cation chloride cotransporters was
249 characterized using aliquots from a prior cohort where the main findings of age, injury, seizure medications, and
250 mechanisms of vasogenic edema had been published. The effect of TBI injuries in humans on cation chloride
251 cotransporters was examined using autopsy samples and semi-quantitatively evaluated by a board-certified
252 forensic neuropathologist (DM).

253 *Statistical analysis*

254 Graphing and statistical analyses were completed in GraphPad Prism. Parametric statistical tests included
255 student's t-test, two- or three-way ANOVA considering age, treatment, co-variates, and/or region as applicable
256 and described in the figure legends. Single variate analysis utilized Pearson correlation and curve fit (R^2) and/or
257 p values are displayed on the graph where applicable. Multivariate analysis was performed when applicable and
258 multiple linear regressions (Pearson's) correlation matrices are displayed on the figure. Exact p values are
259 included on the graphs. For non-parametric data, either Spearman correlation, Mann-Whitney, Wilcoxson Signed
260 Rank Test or Kruskal-Wallis Test by Ranks considering age, treatment, and/or region as applicable were
261 performed as described in the figure legends.

262

263 **RESULTS:**

264 **Establishing the swine "GABA switch" with high spatial and temporal resolution.**

265 We examined the expression and abundance of key chloride cotransporters (*Slc12a2*/NKCC1 and
266 *Slc12a5*/KCC2) and a regulatory kinase (*Stk39/*SPAK) in the American Yorkshire pig (*Sus scrofa domesticus*)
267 across several developmental stages, aiming to map how these changes might align with a prenatal, perinatal,
268 or postnatal GABA switch. In many studies, the relative mRNA expression of these transporters, and a ratio of
269 *Slc12a5 / Scl12a2* have been utilized as a marker for the "GABA switch" (ex. Sedmak et al., 2016).

270 *mRNA expression of Slc12a2, Slc12a5, and Stk39 across development and region in swine*

271 Our intent was to determine whether transcriptional patterns recapitulate those described in other species
272 and to gain initial insight into the developmental timing of the GABA switch in swine. Transcriptional analysis
273 suggests the swine GABA switch occurs perinatally, with region-specific trends in *Slc12a2* (NKCC1) and *Slc12a5*

274 (KCC2) expression differing from altricial species, while *Stk39* (SPAK) levels showed no significant
275 developmental changes.

276 We began by quantifying mRNA expression of *Slc12a2*, *Slc12a5*, and *Stk39* in somatosensory cortex ,
277 hippocampus, and thalamus at embryonic day 36 (ED36), ED90, ED105, postnatal day 7 ("infant"), and postnatal
278 day 30 ("toddler") (**Figure 1A**; demographic data in **1A'**). As shown in **Figures 1B and 1B'**, *Slc12a2* expression
279 remained relatively constant in hippocampus and thalamus, while cortex levels exhibited a moderate upward
280 trend over time. Although these findings were somewhat variable, this complexity may reflect underlying cellular
281 heterogeneity between samples, as NKCC1 is expressed in both neurons and non-neuronal cells (Kurki et al.,
282 2023*)*. For *Slc12a5* (**Figures 1C and 1C'**), expression in the hippocampus and thalamus remained relatively
283 stable, but the cortex showed a marked developmental decrease (Spearman non-parametric R^2=0.89,
284 p=0.0235). This downward cortical trend contrasts with the postnatal increase reported in altricial species,
285 suggesting that, in swine, the GABA switch might occur earlier, closer to birth—more in line with precocial and
286 semi-altricial mammals (Ben-Ari 2014). Lastly, *Stk39* (**Figure 1D and 1D'**) did not show significant age- or region-
287 related trends, indicating that *Stk39* transcript levels may not be the most sensitive indicator of developmental
288 shifts in GABAergic signaling at this age.

289 Taken together, our transcriptional analysis provided initial clues that the swine GABA switch may have
290 a perinatal timing, similar to humans and non-human primates, and differs from the patterns observed in highly
291 altricial species such as rodents (Ben-Ari 2014; Khazipov et al., 2001; Sedmak et al., 2016). However, the
292 complexity and variability in these data demonstrate the limitations of relying solely on transcriptional profiles to
293 resolve developmental changes in chloride cotransporter function. To gain a clearer understanding we next
294 turned to protein-level analyses.

295 *Protein abundances and phosphorylation state for NKCC1, KCC2, and SPAK across development and region in*
296 *swine*

297 In protein-level analyses, we observed age-related increases in KCC2/NKCC1 ratios in swine cortex and
298 hippocampus, stable ratios in the thalamus, and opposite trends in SPAK abundance and phosphorylation.
299 Representative western blots, summarized in **Figure 1E**, reflect consistent findings from multiple technical

300 replicates and mean abundances in each biological replicate group. To provide a clearer overview, we visualized
301 mean abundances and phosphorylation ratios as summary heat maps in **Figures 1F–K**, and we considered
302 established interpretations like the ratio of KCC2/NKCC1 (**Figure 1L**) to better contextualize these changes. We
303 found that in naive swine brain, the dimer band of KCC2 and pKCC2 (~250kDa) was more predominant across
304 all ages, so we quantified that band (Agez et al., 2017).

305 In the cortex, the KCC2/NKCC1 ratio increased with postnatal age (Spearman R^2=0.7253, p=0.0671,
306 **Figure 1L**), aligning with a developmental shift toward inhibitory GABA signaling. However, when examining the
307 ratio of phosphorylated (i.e., "activated") KCC2 to phosphorylated NKCC1, we found no clear age effect. This
308 finding suggests that while overall protein levels of these transporters adjust with development, changes in their
309 phosphorylation states might follow a more complex pattern, potentially influenced by other post-translational
310 modifications of these transporters or other modulators of intraneuronal chloride and is beyond the scope of this
311 study.

312 Regionally, hippocampal KCC2/NKCC1 ratios also increased with age (R^2=0.8784, non-linear fit, **Figure**
313 **1N**), mirroring known patterns in rodent models and underscoring KCC2's essential role in maturing hippocampal
314 neurons. In contrast, thalamic ratios remained stable across the developmental time points examined, perhaps
315 indicating that the switch had occurred earlier than in the hippocampus and cortex (**Figure 1O**). Furthermore,
316 although we observed an overall increase in SPAK abundance with age, its phosphorylation state declined—a
317 dynamic that may reflect evolving regulatory mechanisms as the brain matures.

318 ***Postnatal pNKCC1 downregulation in human hippocampus.***

319 To compare these developmental patterns with those observed in humans, we examined hippocampal
320 samples from infants who died unexpectedly from known causes of death. The study design and tissue validation
321 steps are outlined in **Figure 2A.** Previous transcriptional data from qPCR and microarray studies suggest that
322 the GABA switch in humans occurs around birth in the limbic system and neocortex (Sedmak et al., 2016; Tao
323 et al., 2012; Hyde et al., 2011). Furthermore, evidence from slice electrophysiology, Western blot analysis, and
324 immunolocalization has indicated hyperpolarizing GABA activity in the adult temporal lobe cortex and
325 hippocampus (Huberfeld et al., 2015; Wang et al., 2010; Munoz et al., 2007), which is altered in epilepsies.

326 However, our study offers a more detailed resolution and analysis of the activity state (via phosphorylation) of
327 these cotransporters during the immediate postnatal period in infants with normal brain development.

328 Like our approach in swine, we began by measuring mRNA levels of *Slc12a2, Slc12a5*, and *Stk39* in
329 relation to adjusted postconceptional age (PCA) [gestational age plus postnatal age] and found no significant
330 age regulation. As shown in **Figure 2B**, transcriptional levels of these genes remained relatively stable across
331 postnatal ages, and no positive correlation emerged between the ratio of *Slc12a5/Slc12a2* and PCA (**Figure**
332 **2C**). These transcriptional results indicate that major transcriptional shifts in these transporters are minimal
333 during the postnatal period in humans. Similar to swine, transcriptional variability was low in the hippocampus.

334 We then assessed protein abundances and phosphorylation states in these hippocampal samples. Unlike
335 in swine, both the monomer and dimer band of KCC2 were prominent, so we quantified both bands additively.
336 However, the pKCC2 band was only visualized at the monomer weight in this cohort. We found that while total
337 NKCC1 and KCC2 levels increased with age, the ratio of KCC2/NKCC1 decreased with age (**Figure 2D–G**). In
338 contrast, the phosphorylation state of NKCC1 (p-NKCC1) declined significantly over time, while p-KCC2 levels
339 remained low and unchanged. When we considered the ratio of activated KCC2 to activated NKCC1 (**Figure**
340 **2H**), we found a clear upward trend with increasing age. These results suggest that post-translational
341 modifications—in particular, phosphorylation—may be a key driver of the GABA switch during human postnatal
342 development. The increase in relative KCC2 activation aligns with the gradual shift toward inhibitory GABA
343 signaling that characterizes brain maturation (Watanabe et al., 2019; Kahle et al., 2015).

344 ***TBI injuries in swine affect cation chloride cotransporter transcriptional levels in an age x treatment***
345 ***manner.***

346 We next examined the influence of TBI in piglets at different developmental stages and found that severe
347 TBI induced diverse transcriptional, total protein, and phospho-protein changes to NKCC1, KCC2, and SPAK
348 across regions and ages. Across these analyses, specific age- and injury-related patterns emerged. In the cortex,
349 transcripts for *Slc12a2*, *Slc12a5*, and *Stk39* showed main effects of age or treatment (TBI injuries versus sham
350 injuries), as well as age x treatment interactions in some cases (**Supplemental Figure 1**).

351 ***Spatial transcriptomics reveals tissue subtype-specific alterations in chloride transporter expression***
352 ***and pathway dysregulation following severe TBI in swine.***

353 To assess whether NKCC1 could serve as a novel therapeutic target for traumatic brain injury, we
354 assessed *Slc12a2* and *Slc12a5* expression spatially using the GeoMx platform in injured cortical gray and white
355 matter in a toddler piglet with severe brain injury compared to a sham, **Figure 3A**. **Figure 3B** displays 2-fold
356 changes in transcript abundance for *Slc12a2* and *Slc12a5* relative to sham gray matter from the GeoMx data.
357 We observed a significant increase in *Slc12a2* transcript levels in both sham and injured white matter compared
358 to gray matter, with injured white matter showing the highest expression. This upregulation may reflect the
359 presence of NKCC1 in glial cells of the white matter or in injured axonal projections, as NKCC1 typically localizes
360 to neuronal somas and axon initial segments. In contrast, *Slc12a5* transcript levels decreased in both sham and
361 injured white matter relative to gray matter, with a slight, non-significant reduction in injured white matter
362 compared to sham. This pattern suggests a region-specific downregulation of KCC2 in injured axons, potentially
363 contributing to chloride dysregulation in TBI-affected areas. We find a significant interaction between gene
364 expression, brain region, and injury, indicating differential responses to TBI in cortical gray and white matter for
365 both *Slc12a2* and *Slc12a5* (Three-Way ANOVA, **Figure 3B**). These findings suggest that TBI induces distinct
366 region-specific changes in chloride transporter expression, which may impact chloride balance and
367 excitatory/inhibitory signaling post-injury in toddler piglets.

368 Pathway analyses (**Figures 3C–D**) revealed that TBI-associated changes in gene expression in gyral
369 cortical gray matter encompassed both upregulated pathways related to cellular signaling, neural development,
370 and energy metabolism and downregulated pathways involved in cell adhesion, apoptosis, differentiation, and
371 ion transport. Although neuroinflammatory signatures were mixed and did not meet gene ontology enrichment
372 criteria in these damaged regions, these findings are consistent with known complexities underlying
373 neuroinflammation in TBI pathophysiology. Future exploration of additional regions, ages, and longer recovery
374 intervals will be critical to fully elucidate the molecular drivers of injury progression and identify novel therapeutic
375 targets.

376 ***TBI injuries in swine changes cation chloride cotransporter abundance and phosphorylation across***
377 ***cortex and hippocampus.***

378 Western blotting of cortical lysates (**Figures 4A–C**, quantified in **4D–E**), where the severe spreading
379 hypoxic-ischemic injury is typically most profound revealed that younger, infant piglets with TBI exhibited
380 elevated NKCC1, KCC2, and SPAK protein levels compared to older, “toddler” piglets. NKCC1 phosphorylation
381 (pNKCC1) also increased with TBI injury in both ages, indicating that TBI may influence the functional state of
382 this transporter in younger brains. Additionally, where the dimer of KCC2 and pKCC2 was the prominent band
383 in naive samples, in the TBI samples, the monomer band was equally, or sometimes more, abundant and was
384 distinct in pattern by region (**Figure 4A**). In these quantifications, the band intensities were added together (Agez
385 et al., 2017). This difference in blotting patterns for KCC2 compared to naive animals could be explained by the
386 24-hour anesthesia and intensive care regimens experienced by both sham and TBI injury animals, which was
387 absent in the naive cohort. Even though the piglets were anesthetized using a sedation regimen that largely
388 avoided the GABA receptor, anesthetic effects might still have been present. The significant upregulation of
389 SPAK in infant piglets with TBI, but not toddler piglets, is interesting for two reasons. 1) Our previous work
390 identified that while both ages demonstrate cerebral edema due to TBI, toddler piglets show more vasogenic
391 edema than infant piglets (Hochstetler, Price, et al., 2024). An upregulation of both SPAK and NKCC1 in infant
392 piglets with TBI injuries might be driving evolving cytotoxic edema that does not result in vasogenic edema
393 (Glykys et al., 2017; Zhang et al., 2020). 2) SPAK abundance can be promoted by NFkB signaling (Bhuiyan et
394 al., 2022), which could be activated by either the subarachnoid hemorrhage or cortical impact-induced
395 mechanical stress in this model.

396 In the hippocampus—an area typically spared from hypoxic-ischemic injury in this model—we observed
397 increased NKCC1, KCC2, and SPAK in infant TBI piglets compared to toddler TBI piglets (**Figure 4F**). This
398 suggests that even regions not displaying overt injury can exhibit early changes in chloride transporter
399 expression following TBI. Indeed, structural hippocampus damage might require additional time to manifest
400 beyond the 24-hour paradigm of our study. By contrast, no significant age- or treatment-related changes were
401 detected in the thalamus (**Figure 4G**), underscoring thalamic resiliency to this injury type.

402 These observations provide evidence that TBI influences chloride transporter expression and activation
403 differently across brain regions and developmental stages. Younger piglets appear more prone to TBI-related
404 shifts in these key ionic regulators, raising the possibility that early therapeutic interventions targeting chloride
405 cotransporters could be beneficial.

406 ***Severe TBI in swine produces region- and cell-type specific alterations in pNKCC1 that are correlated***
407 ***with damage, subarachnoid hemorrhage, and seizure duration.***

408 TBI significantly increased pNKCC1 expression in non-parvalbumin-expressing cortical neurons
409 ($NeuN^+/pNKCC1^+/PV^-$) of infant piglets positively correlated with seizure duration and SAH area, while cortical
410 PV^+ populations and hippocampal neuronal populations showed no significant changes, indicating region- and
411 cell-specific effects. We utilized immunohistochemistry to assess phosphorylated NKCC1 (pNKCC1) expression
412 in NeuN co-labeled mature neurons in the somatosensory cortex layer 4, revealing more age-specific effects of
413 injury (**Figure 5A**). Apoptotic neurons (**Supplemental Figure 2A**, assessed by nuclear chromatin condensation
414 via Hoechst/$NeuN^+$) in gyral layer 4 increased in toddlers but not infants (**Figure 5B).** Also in gyral layer 4, in the
415 remaining healthy $NeuN^+$ neurons, pNKCC1 counts increased in infants but not toddlers (**Figure 5B**). There was
416 no effect of age nor injury on the number of pNKCC1 in all $NeuN^+$ neurons in the dorsal or ventral hippocampus
417 dentate gyrus or CA2 **(Figure 5C)**. In all hippocampal regions, less than 5% of total neurons were apoptotic
418 (**Supplemental Figure 2B**).

419 In gyral cortical neurons, TBI significantly increased pNKCC1 expression (main effect of treatment
420 p=0.0017, **Figure 5B**). When comparing pNKCC1 levels to univariate injury metrics, **visualized in Figure 5D**/**E**,
421 seizure duration, % damage, and SAH show positive correlation with pNKCC1 in infant piglets (Pearson
422 R^2=0.838, p=0.0093, Spearman R^2=0.833, p=0.0738; Pearson R^2=0.6514, p=0.0801; respectively, **Figure 5E**)
423 Multivariate analysis further confirmed the relationship between neuronal-pNKCC1 expression and SAH% and
424 seizure duration as positive predictors across both ages (**Figure 5F**).

425 Further cell-specific analyses indicated that PV^+ interneurons did not show enhanced pNKCC1 after TBI,
426 suggesting that these inhibitory interneurons remain relatively unaffected. Non-neuronal cells in the cortex
427 displayed nominal, heterogeneous changes in pNKCC1. In the hippocampus, no significant pNKCC1 changes

428 were detected in either neuronal or non-neuronal populations, indicating a regionally selective effect of TBI on
429 pNKCC1 expression. Collectively, these data suggest that TBI-induced elevations in pNKCC1 predominantly
430 occur in surviving cortical PV^- neurons of younger piglets, possibly contributing to a pro-excitatory state
431 associated with seizures.

432 NKCC1 expression is also high in the choroid plexus of many mammals, including piglets. We observed
433 pNKCC1 downregulation and signal fragmentation in the choroid plexus due to severe TBI (**Figure 6A**). We
434 denote signal fragmentation as an ectopic, non-apical pNKCC1 signal in the epithelial cells, indicating the
435 presence, but potential lack of function, of this transporter. This is in opposition to a prior study where rats with
436 cortical contusion injuries showed an upregulation of NKCC1 in the choroid plexus within 24 hours following
437 injury (Lu et al., 2006). Two factors may explain this result. The first is the severity of the injury, where the rats
438 with contusion injuries were a much less severe model than our piglet model, which requires intensive care to
439 sustain. The second factor is age, where our piglet model is accomplished in young animals, the rat model
440 utilized adult animals.

441 ***Region- and cell-type-specific alterations in pNKCC1 expression are heterogeneous in an autopsy series***
442 ***of pediatric TBI.***

443 To bridge our findings from the piglet model to humans, we examined pNKCC1 expression in autopsy
444 samples from non-TBI and TBI cases covering a range of ages (detailed neuropathological findings in
445 **Supplemental File 1**). In control, human tissue, pNKCC1 was consistently present at low to moderate levels in
446 neurons and glia across multiple regions, with relatively robust expression in ependyma and choroid plexus. In
447 TBI cases, pNKCC1 expression varied according to injury severity and location. Regions with significant hypoxic-
448 ischemic damage, including the parietal lobe, corpus callosum, and hippocampus, showed increased pNKCC1
449 in glia and axons relative to controls. The temporal lobe, especially ependyma of the striatum terminalis, exhibited
450 pronounced pNKCC1 upregulation in cases with severe white matter injuries. Meanwhile, the choroid plexus
451 demonstrated reduced pNKCC1 expression, mirroring signal fragmentation patterns seen in piglets (**Figure 6B**).
452 In human cases, profound damage to the choroid plexus (temporal lobe, lateral ventricle) accompanied this

453 phenomenon. The atrium of the lateral ventricle was chosen in the piglets as a match for the human cases due
454 to the proximity to the hippocampus.

455 These human data align closely with the piglet findings, suggesting that TBI prompts region- and cell-
456 specific changes in chloride transporter phosphorylation. The parallels in pNKCC1 distribution and injury-related
457 shifts point toward a conserved mechanism by which TBI alters ionic balance and potentially contributes to
458 secondary injury processes in the developing brain in neurons that survive the brain injury.

459

460 **DISCUSSION:**

461 A central feature of normal brain development is the "GABA switch," in which inhibitory transduction
462 matures as the balance shifts from NKCC1-driven chloride influx toward KCC2-mediated chloride efflux. This
463 switch helps mature neural circuits, limit hyperexcitability, and prevent seizures. Our swine data show that this
464 switch occurs around the perinatal period in a pattern more closely resembling semi-altricial species (including
465 primates) than altricial rodents. In humans, we similarly observed a gradual postnatal decrease in NKCC1
466 phosphorylation aligned with a relative increase in potential inhibitory tone over time. Together, these findings
467 suggest that swine provide a useful experimental bridge for modeling human neurodevelopment and the timing
468 of the GABA switch.

469 We hypothesized that regions of tissue damage (i.e. cerebral cortex) would exhibit changes to the
470 NKCC1/KCC2 balance and regions without tissue damage (hippocampus and thalamus) would not. We did find
471 upregulation of NKCC1 in the cortex as predicted, but we also found changes in hippocampus as well, a region
472 which does not have acute tissue damage in our model at the 24 post-injury timepoint, but perhaps would exhibit
473 structural damage chronically (Costine-Bartell et al., 2019). We saw no change to transporter abundance in
474 thalamus, an area we expect to be spared in our model both acutely and chronically as the thalamus is spared
475 in children with Hemispheric Hypodensity (Durham and Duhaime 2007).

476 We further hypothesized that toddler piglets with more pervasive, hemispheric spreading injury with and
477 more pronounced vasogenic edema would exhibit upregulated NKCC1 compared to infant piglets with patchy,
478 less tissue damage. However, we found the opposite to be true where greater upregulation of NKCC1 and SPAK

479 in response to injury was not in the age with greater tissue damage. Younger animals displayed a more
480 pronounced TBI-induced upregulation of NKCC1 and SPAK, a kinase that promotes NKCC1 phosphorylation
481 and activity. This shift toward elevated NKCC1 function can increase neuronal excitability and seizure risk—
482 clinical challenges frequently observed in pediatric TBI. This is perhaps because apoptotic (dead) neurons,
483 perhaps due to cytotoxic edema, which are abundant in the injured toddler piglets, are non-functional and will
484 not be affected by changes to the Cl^- milieu, whereas surviving neurons might exhibit ongoing dysfunction. The
485 correlation between pNKCC1 counts and seizure duration and hemorrhage in piglets further reinforces the notion
486 that disrupted chloride regulation might contribute to excitatory/inhibitory imbalances after injury. Notably, these
487 TBI-induced changes were not uniform across cell types or regions: parvalbumin-positive cortical interneurons
488 were spared, and hippocampal neurons remained relatively unaffected by these specific injuries. Since
489 hippocampal neurons didn't show significantly increased neuronal-pNKCC1, but lysates showed upregulated
490 NKCC1, perhaps non-neuronal NKCC1 upregulation contributes to early responses to TBI before neuron
491 dysfunction. Moreover, changes in chloride transporter expression extended beyond neurons and non-neuronal
492 cortical cells, such as the downregulation in the choroid plexus. Spatial transcriptomics indicated that white
493 matter alterations in NKCC1 and KCC2 expression likely involve glial cells and support matrix, influencing
494 extracellular ion balance and potentially contributing to edema and barrier dysfunction. Indeed, we previously
495 demonstrated that toddlers, which have the most damage, also have ongoing upregulation in abundance and
496 activity of matrix metalloproteinase, whereas matrix metalloproteinases are either not increased or even
497 downregulated in infants, who have less damage (Hochstetler et al., 2024). This works supports the hypothesis
498 that chloride transporters alone do not control intraneuronal chloride concentrations, especially after pediatric
499 TBI (Normoyle et al., 2024). Human autopsy data corroborated these animal findings. In TBI cases, we saw
500 similar region- and cell-type-specific shifts in pNKCC1, particularly in damaged white matter tracts and in the
501 choroid plexus. We believe this dysregulation of choroidal pNKCC1 signal could likely be a consequence of
502 severe injury, including hemorrhages into the CSF space – specifically subarachnoid hemorrhage (SAH) and
503 intraventricular hemorrhage (IVH), and perhaps CSF production by choroid plexus transporters is shunted. An
504 alternative explanation could be that the choroid plexus is mechanically damaged in our injury model and in

505 severe TBI in humans. Together, our finding of choroid plexus pNKCC1 dysregulation demonstrates how severe
506 TBI disturbs ionic homeostasis at brain-fluid interfaces, potentially affecting cerebrospinal fluid dynamics, cell
507 volume, bulk tissue shifts, and intracranial pressure.

508 Taken together, after TBI, toddler piglets display vasogenic edema likely from MMP upregulation, while
509 infant piglets might instead experience acute cytotoxic edema with rapid, clean cell death without leading to
510 vasogenic edema, resulting in ongoing neuronal dysfunction in surviving neurons, which might make them
511 unique candidates for therapeutic intervention (Balena and Staley, 2024). This postulate is supported by Level
512 III clinical evidence and recent age-dependent mechanisms of cerebral edema in small diameter blood vessels
513 following severe TBI in an autopsy case-series investigation (Fullerton et al., 2021). Given the robust age- and
514 treatment-effects of TBI injuries on SPAK abundance, we propose that treatment of our infant piglets with a
515 SPAK inhibitor immediately following TBI might offer protective and antiepileptic effects (Gong et al., 2021; Wu
516 et al. 2020). Indeed, as pathophysiology is age-specific, successful therapeutics might also need to be age-
517 specific after severe TBI according to developmental stage: targeting NKCC1 or SPAK in infants and targeting
518 MMP's in toddlers.

519 *Limitations:*

520 Our study has several limitations that should be acknowledged. Firstly, we were not powered to examine
521 the distinct effect of sex as a covariate on NKCC1 and KCC2 levels in the developing swine brain due to protocol
522 limitations, which may influence the observed outcomes (Missios et al., 2009). Additionally, we did not assess
523 the levels of brain-derived neurotrophic factor (BDNF) or insulin-like growth factor (IGF), both of which are known
524 to promote the GABA switch. Other intracellular regulators such as protein kinase C (PKC), Src kinases, and
525 with no-lysine (WNK) kinases, the latter of which are chloride-sensitive and may play a role in the switch, were
526 also not considered in this study (Watanabe and Fukuda 2015). Furthermore, we did not investigate the potential
527 contributions of maternal estrogen or taurine as positive sensory regulators of the GABA switch. Finally, and
528 perhaps most importantly, we did not perform electrophysiology or chloride ion imaging either *in vivo* or in
529 organotypic slice, thus, our observations are limited to when the switch is *likely* occurring, however, we cannot
530 say with certainty when GABA switches from excitatory to inhibitory in the developing swine brain.

531 Our study, while leveraging a translationally relevant swine model and human autopsy samples, cannot
532 fully capture the clinical complexity and heterogeneity of pediatric TBI. The standardized injury approach in pigs,
533 though informative, may not reflect the multifaceted trauma mechanisms, variable interventions, and long
534 recovery trajectories seen in patients. These factors represent important avenues for future research to better
535 understand the mechanisms underlying the excitatory/inhibitory balance in the developing swine brain and in the
536 context of TBI. Donnan effects with the loss of the extracellular matrix also likely affect the amount of
537 extraneuronal and intraneuronal chloride concentrations post-TBI as demonstrated in rodent hippocampal
538 explants (Glykys et al., 2014; Normoyle et al., 2024). Indeed, in our own severe TBI model, we have described
539 an age-dependent upregulation of matrix metalloproteinases where there was an ongoing upregulation in
540 toddlers with worse injury, compared to a resolution in infants with lower injury burden scaled to brain volume.
541 The human autopsy samples, while invaluable, represent end-stage conditions and lack information on the
542 temporal progression of TBI pathology. Further, it is unclear to what extent non-traumatic pediatric autopsy
543 samples are representative of a physiologically normal pediatric population.

544 We observed notable variability in transcript-level measurements, likely due to biological heterogeneity
545 and technical factors such as RNA quality, sampling consistency, and cellular composition of lysates. Though
546 immunoblotting analyses were particularly informative, phosphorylation state was less informative in swine. It is
547 important to note that our study did not evaluate additional post-translational modifications, such as glycosylation,
548 though these are certainly indicated in the activity of these transporters. Finally, while we identified potential
549 mechanistic links between chloride transporter dysregulation, seizures, and injury severity, further studies are
550 needed to establish causal relationships and to explore how interventions that target these pathways might
551 improve long-term outcomes in pediatric TBI.

552 *Conclusions and future directions:*

553 By integrating findings from a swine model—whose brain development and structure closely parallel
554 those of humans—with postmortem human tissue analyses, our work supports the translational value of targeting
555 chloride regulation to improve TBI outcomes, especially in pediatric populations (Glykys et al., 2017; Soul et al.,
556 2021; Staley 2022). Pharmacologically modulating NKCC1 or KCC2—potentially with agents like bumetanide or

a SPAK inhibitor—could help restore chloride homeostasis and reduce hyperexcitability and swelling/tissue shifts after pediatric TBI. Such treatments would need to consider the patient's developmental stage and the specific brain regions affected. Early intervention, when the brain is most vulnerable to ionic imbalances, may be especially beneficial. Our findings emphasize that TBI's impact on the developing brain cannot be fully understood by focusing solely on neuronal excitability or a single brain area. Instead, we must consider a dynamic interplay among developmentally regulated ion transporters, glial function, neuroinflammatory processes, and structural integrity. Future work should address 1) how these factors interact over longer recovery periods, potentially via *in vivo* monitoring of neuronal chloride (Costine-Bartell et al., 2023), 2) explore targeted therapies that normalize chloride balance, and 3) consider how interventions might influence long-term neurodevelopmental outcomes and post-traumatic sequelae such as epilepsy.

568 **References**:

569

570 Agez M, Schultz P, Medina I, Baker DJ, Burnham MP, Cardarelli RA, Conway LC, Garnier K, Geschwindner S, Gunnarsson
571 A, McCall EJ, Frechard A, Audebert S, Deeb TZ, Moss SJ, Brandon NJ, Wang Q, Dekker N, Jawhari A. (2017) Molecular
572 architecture of potassium chloride co-transporter KCC2. Sci Rep. Nov 28;7(1):16452.

573 Balena T, Staley K. (2024). Neuronal Death: Now You See It, Now You Don't. Neuroscientist. Sep 24:10738584241282632.

574 Ben-Ari Y, Gaiarsa JL, Tyzio R, Khazipov R. (2007). GABA: a pioneer transmitter that excites immature neurons and
575 generates primitive oscillations. Physiol Rev. Oct;87(4):1215-84.

576 Ben-Ari Y. (2014). The GABA excitatory/inhibitory developmental sequence: a personal journey. Neuroscience. Oct
577 24;279:187-219.

578 Bhuiyan MIH, Young CB, Jahan I, Hasan MN, Fischer S, Meor Azlan NF, Liu M, Chattopadhyay A, Huang H, Kahle KT,
579 Zhang J, Poloyac SM, Molyneaux BJ, Straub AC, Deng X, Gomez D, Sun D. (2022) NF-κB Signaling-Mediated Activation
580 of WNK-SPAK-NKCC1 Cascade in Worsened Stroke Outcomes of Ang II-Hypertensive Mice. Stroke. May;53(5):1720-1734.

581 Bienboire-Frosini C, Marcet-Rius M, Orihuela A, Domínguez-Oliva A, Mora-Medina P, Olmos-Hernández A, Casas-Alvarado
582 A, Mota-Rojas D. (2023) Mother-Young Bonding: Neurobiological Aspects and Maternal Biochemical Signaling in Altricial
583 Domesticated Mammals. Animals (Basel). Feb 2;13(3):532

584 Bortone D, Polleux F. (2009). KCC2 expression promotes the termination of cortical interneuron migration in a voltage-
585 sensitive calcium-dependent manner. Neuron. Apr 16;62(1):53-71.

586 Clancy B, Finlay BL, Darlington RB, Anand KJ. (2007). Extrapolating brain development from experimental species to
587 humans. Neurotoxicology. Sep;28(5):931-7.

588 Costine-Bartell B, Price G, Shen J, McGuone D, Staley K, Duhaime AC. (2021). A perfect storm: The distribution of tissue
589 damage depends on seizure duration, hemorrhage, and developmental stage in a gyrencephalic, multi-factorial, severe
590 traumatic brain injury model. Neurobiol Dis. Jul;154:105334.

591 Costine-Bartell BA, Martinez-Ramirez L, Normoyle K, Stinson T, Staley KJ, Lillis KP. (2023). 2-photon imaging of fluorescent
592 proteins in living swine. Sci Rep. Aug 29;13(1):14158.

593 Costine-Bartell BA, McGuone D, Price G, Crawford E, Keeley KL, Munoz-Pareja J, Dodge CP, Staley K, Duhaime AC.
594 (2019). Development of a Model of Hemispheric Hypodensity ("Big Black Brain"). J Neurotrauma. Mar 1;36(5):815-833.

595 Dobbin J and Sands J. (1979) Early Human Development. Vol. 311 Pages 79-83.

596 Duhaime AC, Durham S. (2007) Traumatic brain injury in infants: the phenomenon of subdural hemorrhage with hemispheric
597 hypodensity ("Big Black Brain") Prog Brain Res. 161:293-302.

598 Foster KA, Recker M, Lee P, Bell MJ, Tyler-Kabara E. (2014) Factors Associated with Hemispheric Hypodensity after
599 Subdural Hematoma following Abusive Head Trauma in Children. J Neurotrauma. 2014 Oct 1;31(19):1625-31.

600 Fullerton JL, Hay J, Bryant-Craig C, Atkinson J, Smith DH, Stewart W. (2024) Pediatric Traumatic Brain Injury and
601 Microvascular Blood-Brain Barrier Pathology. JAMA Netw Open. Nov 4;7(11):e2446767.

602 Glykys J, Dzhala V, Egawa K, Balena T, Saponjian Y, Kuchibhotla KV, Bacskai BJ, Kahle KT, Zeuthen T, Staley KJ. (2014)
603 Local impermeant anions establish the neuronal chloride concentration. Science. Feb 7;343(6171):670-5.

604 Glykys J, Dzhala V, Egawa K, Kahle KT, Delpire E, Staley K. (2017) Chloride Dysregulation, Seizures, and Cerebral Edema:
605 A Relationship with Therapeutic Potential. Trends Neurosci. May;40(5):276-294.

606 Goldstein RD, Poduri A. (2024) Seizures and Sudden Death Beyond SUDEP. Neurology. Feb 13;102(3):e208119.

Gong Y, Wu M, Gao F, Shi M, Gu H, Gao R, Dang BQ, Chen G. (2021) Inhibition of the p-SPAK/p-NKCC1 signaling pathway protects the blood-brain barrier and reduces neuronal apoptosis in a rat model of surgical brain injury. Mol Med Rep. Oct;24(4):717.

Harowitz J, Crandall L, McGuone D, Devinsky O. (2021) Seizure-related deaths in children: The expanding spectrum. Epilepsia. Mar;62(3):570-582.

Haynes RL, Kinney HC, Haas EA, Duncan JR, Riehs M, Trachtenberg F, Armstrong DD, Alexandrescu S, Cryan JB, Hefti MM, Krous HF, Goldstein RD, Sleeper LA. (2021) Medullary Serotonergic Binding Deficits and Hippocampal Abnormalities in Sudden Infant Death Syndrome: One or Two Entities? Front Pediatr. Dec 21;9:762017.

Hochstetler A, Price G, Baohan A, Li M, Rodriguez Lara F, Lok J, Costine-Bartell B. (2024). Developmental Regulation of Matrix Metalloproteinases in Response to Multifactorial, Severe Traumatic Brain Injuries during Immaturity. Dev Neurosci. 46(5):319-332.

Huberfeld G, Blauwblomme T, Miles R. (2015) Hippocampus and epilepsy: Findings from human tissues. Rev Neurol (Paris). Mar;171(3):236-51.

Hyde TM, Lipska BK, Ali T, Mathew SV, Law AJ, Metitiri OE, Straub RE, Ye T, Colantuoni C, Herman MM, Bigelow LB, Weinberger DR, Kleinman JE. (2011) Expression of GABA signaling molecules KCC2, NKCC1, and GAD1 in cortical development and schizophrenia. J Neurosci. Jul 27;31(30):11088-95.

Ibrahim NG, Natesh R, Szczesny SE, Ryall K, Eucker SA, Coats B, Margulies SS. (2010). In situ deformations in the immature brain during rapid rotations. J Biomech Eng. Apr;132(4):044501.

Kahle KT, Deeb TZ, Puskarjov M, Silayeva L, Liang B, Kaila K, Moss SJ. (2013) Modulation of neuronal activity by phosphorylation of the K-Cl cotransporter KCC2. Trends Neurosci. Dec;36(12):726-737.

Keenan HT, Runyan DK, Marshall SW, Nocera MA, Merten DF, Sinal SH. (2003). A population-based study of inflicted traumatic brain injury in young children. JAMA. Aug 6;290(5):621-6.

Khazipov R, Esclapez M, Caillard O, Bernard C, Khalilov I, Tyzio R, Hirsch J, Dzhala V, Berger B, Ben-Ari Y. (2001) Early development of neuronal activity in the primate hippocampus in utero. J Neurosci. Dec 15;21(24):9770-81.

Kurki SN, Uvarov P, Pospelov AS, Trontti K, Hübner AK, Srinivasan R, Watanabe M, Hovatta I, Hübner CA, Kaila K, Virtanen MA. (2023). Expression patterns of NKCC1 in neurons and non-neuronal cells during cortico-hippocampal development. Cereb Cortex. May 9;33(10):5906-5923.

Leitner DF, William C, Faustin A, Askenazi M, Kanshin E, Snuderl M, McGuone D, Wisniewski T, Ueberheide B, Gould L, Devinsky O. (2022) Proteomic differences in hippocampus and cortex of sudden unexplained death in childhood. Acta Neuropathol. May;143(5):585-599.

Lind NM, Moustgaard A, Jelsing J, Vajta G, Cumming P, Hansen AK. (2007). The use of pigs in neuroscience: modeling brain disorders. Neurosci Biobehav Rev. 31(5):728-51.

LoTurco JJ, Owens DF, Heath MJ, Davis MB, Kriegstein AR. (1995). GABA and glutamate depolarize cortical progenitor cells and inhibit DNA synthesis. Neuron. Dec;15(6):1287-98.

Lu KT, Wu CY, Cheng NC, Wo YY, Yang JT, Yen HH, Yang YL. (2006). Inhibition of the Na+ -K+ -2Cl- -cotransporter in choroid plexus attenuates traumatic brain injury-induced brain edema and neuronal damage. Eur J Pharmacol. Oct 24;548(1-3):99-105. doi: 10.1016/j.ejphar.2006.07.048.

Missios S, Harris BT, Dodge CP, Simoni MK, Costine BA, Lee YL, Quebada PB, Hillier SC, Adams LB, Duhaime AC. (2009). Scaled cortical impact in immature swine: effect of age and gender on lesion volume. J Neurotrauma. Nov;26(11):1943-51.

Muñoz A, Méndez P, DeFelipe J, Alvarez-Leefmans FJ. (2007) Cation-chloride cotransporters and GABA-ergic innervation in the human epileptic hippocampus. Epilepsia. Apr;48(4):663-73.

Normoyle KP, Lillis KP, Egawa K, McNally MA, Paulchakrabarti M, Coudhury BP, Lau L, Shiu FH, Staley KJ. (2024) Displacement of extracellular chloride by immobile anionic constituents of the brain's extracellular matrix. J Physiol. Dec 2.

Patodia S, Somani A, Thom M. (2021) Review: Neuropathology findings in autonomic brain regions in SUDEP and future research directions. Auton Neurosci. Nov;235:102862.

Peerboom C, Wierenga CJ. (2021). The postnatal GABA shift: A developmental perspective. Neurosci Biobehav Rev. May;124:179-192.

Sauro KM, Wiebe S, Dunkley C, Janszky J, Kumlien E, et al. 2016. The current state of epilepsy guidelines: A systematic review. Epilepsia 57: 13-23

Sedmak G, Jovanov-Milošević N, Puskarjov M, Ulamec M, Krušlin B, Kaila K, Judaš M. (2016) Developmental Expression Patterns of KCC2 and Functionally Associated Molecules in the Human Brain. Cereb Cortex. Dec;26(12):4574-4589.

Smith DM, McGinnis EL, Walleigh DJ, Abend NS. 2016. Management of Status Epilepticus in Children. J Clin Med 5.

Soul JS, Bergin AM, Stopp C, Hayes B, Singh A, Fortuno CR, O'Reilly D, Krishnamoorthy K, Jensen FE, Rofeberg V, Dong M, Vinks AA, Wypij D, Staley KJ; Boston Bumetanide Trial Group. (2021) A Pilot Randomized, Controlled, Double-Blind Trial of Bumetanide to Treat Neonatal Seizures. Ann Neurol. Feb;89(2):327-340.

Staley KJ. (2022) Clarifications regarding bumetanide for neonatal seizures. Epilepsia. Jul;63(7):1863-1867. doi: 10.1111/epi.17278. Epub 2022 May 26.

Swindle MM, Smith AC, Hepburn BJ. (1988). Swine as models in experimental surgery. J Invest Surg. 1(1):65-79.

Tang BL. (2020) The Expanding Therapeutic Potential of Neuronal KCC2. Cells. Jan 17;9(1):240.

Tao R, Li C, Newburn EN, Ye T, Lipska BK, Herman MM, Weinberger DR, Kleinman JE, Hyde TM. (2012) Transcript-specific associations of SLC12A5 (KCC2) in human prefrontal cortex with development, schizophrenia, and affective disorders. J Neurosci. Apr 11;32(15):5216-22.

Wang WZ, Hoerder-Suabedissen A, Oeschger FM, Bayatti N, Ip BK, Lindsay S, Supramaniam V, Srinivasan L, Rutherford M, Møllgård K, Clowry GJ, Molnár Z. (2010) Subplate in the developing cortex of mouse and human. J Anat. Oct;217(4):368-80.

Watanabe M, Fukuda A. (2015) Development and regulation of chloride homeostasis in the central nervous system. Front Cell Neurosci. Sep 24;9:371.

Watanabe M, Zhang J, Mansuri MS, Duan J, Karimy JK, Delpire E, Alper SL, Lifton RP, Fukuda A, Kahle KT. (2019). Developmentally regulated KCC2 phosphorylation is essential for dynamic GABA-mediated inhibition and survival. Sci Signal. Oct 15;12(603):eaaw9315.

Wu D, Lai N, Deng R, Liang T, Pan P, Yuan G, Li X, Li H, Shen H, Wang Z, Chen G. (2020) Activated WNK3 induced by intracerebral hemorrhage deteriorates brain injury maybe via WNK3/SPAK/NKCC1 pathway. Exp Neurol. Oct;332:113386.

Young JW, Mayerl CJ, Mannava A, Lewis C, Fan T, Nair M, Mamone C, Schapker NM, Mossor AM, German RZ. (2023) Evaluating The Precocial-altricial Axis of Motor Skill at Birth in A Preterm Pig Model. Integr Comp Biol. Sep 15;63(3):625-640.

Zhang J, Bhuiyan MIH, Zhang T, Karimy JK, Wu Z, Fiesler VM, Zhang J, Huang H, Hasan MN, Skrzypiec AE, Mucha M, Duran D, Huang W, Pawlak R, Foley LM, Hitchens TK, Minnigh MB, Poloyac SM, Alper SL, Molyneaux BJ, Trevelyan AJ, Kahle KT, Sun D, Deng X. (2020) Modulation of brain cation-Cl- cotransport via the SPAK kinase inhibitor ZT-1a. Nat Commun. Jan 7;11(1):78.

Figure 1:

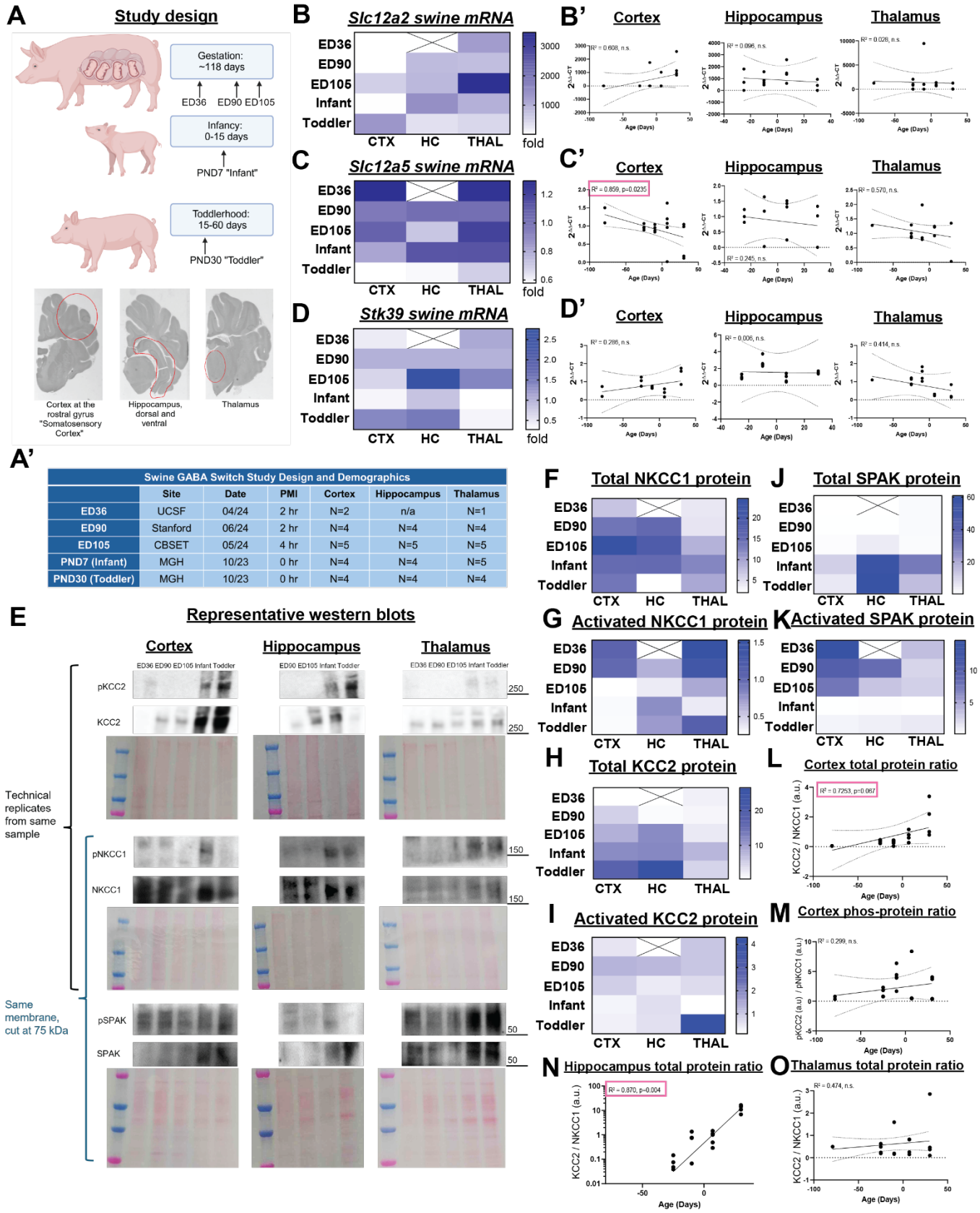
A
Study design
Gestation: ~118 days
ED36 ED90 ED105
Infancy: 0-15 days
PND7 "Infant"
Toddlerhood: 15-60 days
PND30 "Toddler"
Cortex at the rostral gyrus "Somatosensory Cortex"
Hippocampus, dorsal and ventral
Thalamus
B
Slc12a2 swine mRNA
C
Slc12a5 swine mRNA
D
Stk39 swine mRNA
ED36
ED90
ED105
Infant
Toddler
CTX HC THAL
fold
B' Cortex Hippocampus Thalamus
C' Cortex Hippocampus Thalamus
D' Cortex Hippocampus Thalamus
Age (Days)
A'
Swine GABA Switch Study Design and Demographics
Site Date PMI Cortex Hippocampus Thalamus
ED36 UCSF 04/24 2 hr N=2 n/a N=1
ED90 Stanford 06/24 2 hr N=4 N=4 N=4
ED105 CBSET 05/24 4 hr N=5 N=5 N=5
PND7 (Infant) MGH 10/23 0 hr N=4 N=4 N=5
PND30 (Toddler) MGH 10/23 0 hr N=4 N=4 N=4
E
Representative western blots
Cortex Hippocampus Thalamus
ED36 ED90 ED105 Infant Toddler
pKCC2
KCC2
pNKCC1
NKCC1
pSPAK
SPAK
Technical replicates from same sample
Same membrane, cut at 75 kDa
F Total NKCC1 protein
J Total SPAK protein
G Activated NKCC1 protein
K Activated SPAK protein
H Total KCC2 protein
L Cortex total protein ratio
I Activated KCC2 protein
M Cortex phos-protein ratio
N Hippocampus total protein ratio
O Thalamus total protein ratio
KCC2 / NKCC1 (a.u.)
pKCC2 (a.u.) / pNKCC1 (a.u.)

Figure 1: The expression of KCC2 in cortex and hippocampus matures postnatally in the developing swine brain.

A, study design, sample acquisition (***A'***), and approximate age of swine across the developmental axis. ***B***, expression of *Slc12a2* across development and region in swine presented as heat map for mean fold change relative to ED90. All data points presented in ***B'***. ***C***, expression of *Slc12a5* across development and region in swine presented as heat map for mean fold change relative to ED90. All data points presented in ***C'***. ***D***, expression of *Stk39* across development and region in swine presented as heat map for mean fold change relative to ED90. All data points presented in ***D'***. ***E***, representative western blots for each protein with total protein stain presented as loading control. ***F***, NKCC1 protein presented as heat map for mean a.u. normalized to total protein across developmental ages and regions. ***G***, phosphorylated NKCC1 protein presented as heat map for mean pNKCC1 a.u. normalized to total NKCC1 across developmental ages and regions. ***H***, KCC2 protein presented as heat map for mean a.u. normalized to total protein across developmental ages and regions. ***I***, phosphorylated KCC2 protein presented as heat map for mean pKCC2 a.u. normalized to KCC2 a.u. across developmental ages and regions. ***H***, SPAK protein presented as heat map for mean a.u. normalized to total protein across developmental ages and regions. ***I***, phosphorylated SPAK protein presented as heat map for mean pSPAK a.u. normalized to SPAK a.u. across developmental ages and regions. ***L***, Ratio of KCC2/NKCC1 in cortex over development. ***M***, Ratio of phosphoKCC2/phosphoNKCC1 in cortex over development. ***N***, Ratio of KCC2/NKCC1 in hippocampus over development. ***O***, Ratio of KCC2/NKCC1 in thalamus over development. For all correlative relationships, significant findings (Pearson or nonlinear fit) are noted on the graphs with a pink box and Pearson fits and 95% Confidence interval bands are shown for all.

Figure 2:

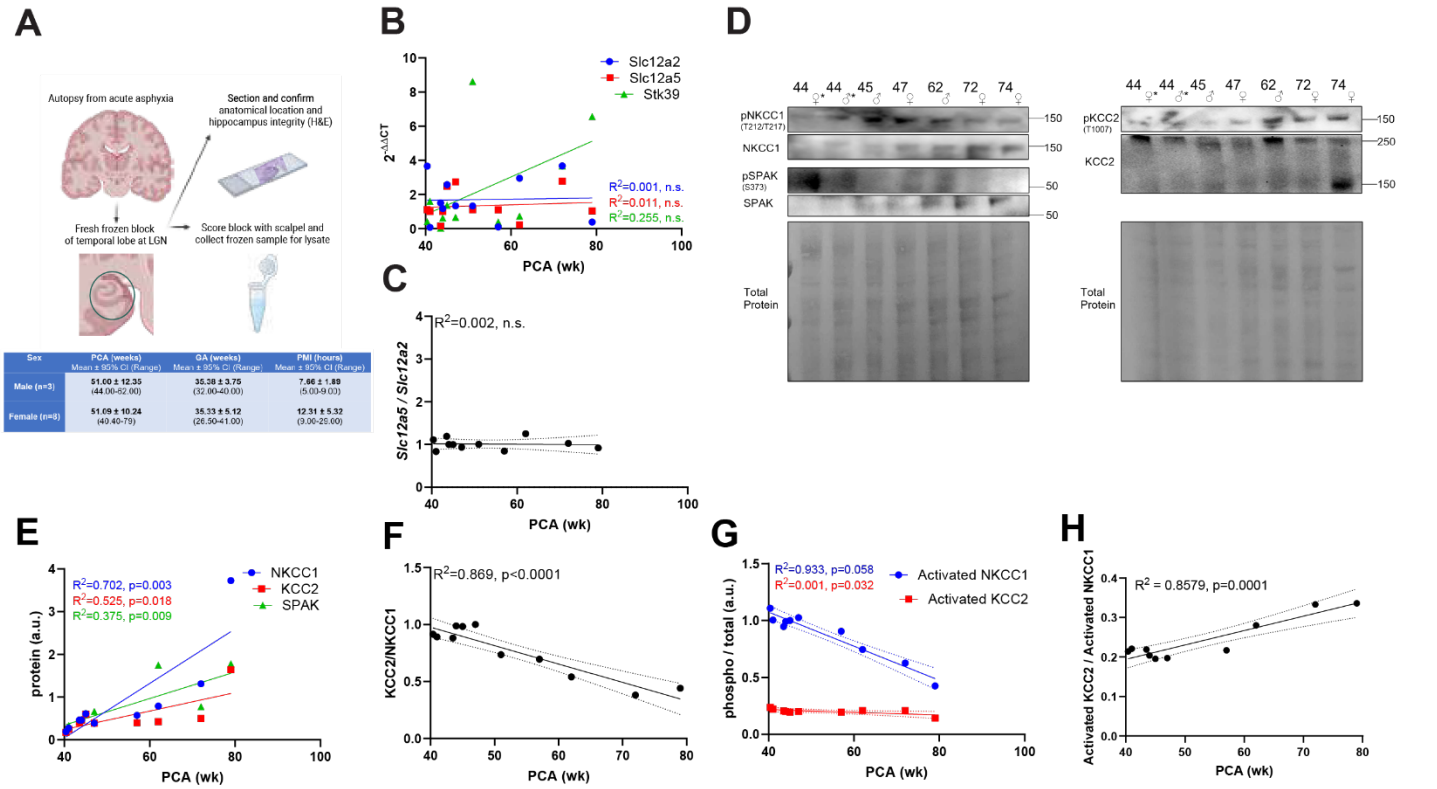

Figure 2: Phosphorylated KCC2 increases with postnatal age in human hippocampus. ***A***, study design, acquisition, and demographics of fresh frozen infantile human hippocampus samples. ***B***, expression of *Slc12a2*, *Slc12a5*, and *Stk39* over postnatal development. ***C***, Ratio of *Slc12a5/Slc12a2* transcript over postnatal development. ***D***, representative western blots from selected samples showing protein abundance over developmental age with total protein stain as loading control. ***E***, Protein abundances for NKCC1, KCC2, and SPAK graphed over age for all samples. ***F***, Abundance of KCC2 / NKCC1 over postnatal age. ***G***, Ratio of phosphorylated to total protein over developmental age for NKCC1 and KCC2. ***H***, Ratio of activated KCC2 / activated NKCC1 plotted over developmental age. For all linear relationships, Pearson correlations are noted on the graphs and 95% Confidence interval bands are shown.

723 **Figure 3:**

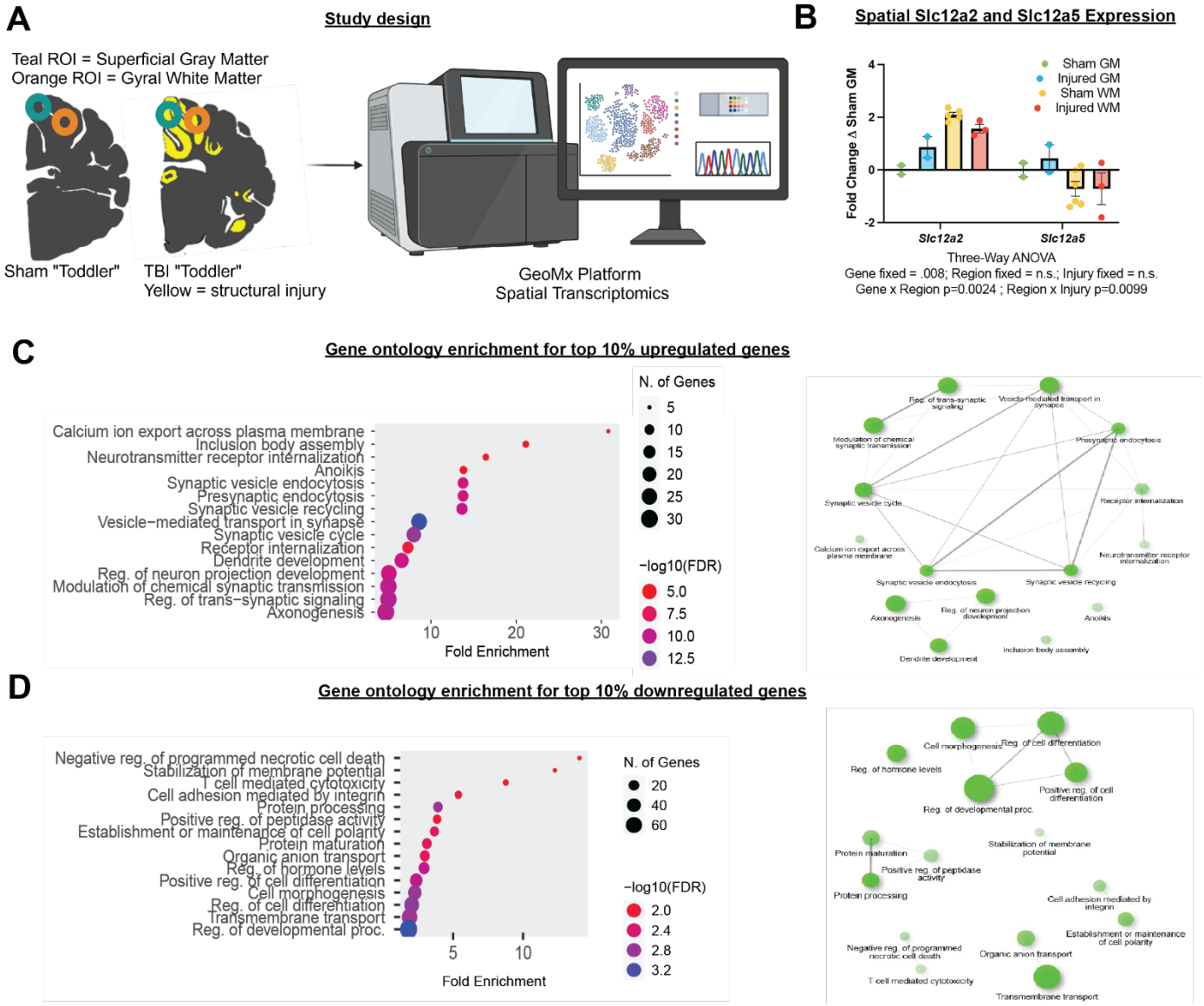

724

725 **Figure 3: Spatial transcriptomic profiling of toddler piglets reveals region- and injury- specific changes**
726 **to *Slc12a2* and *Slc12a5* and identifies mechanisms of ongoing tissue damage.**
727 ***A***, Study design and ROI selection for GeoMx Spatial Transcriptomics. ***B***, Selected relative expression of
728 *Slc12a2* (encoding NKCC1) and *Slc12a5* (encoding KCC2) across regions from sham animals and animals with
729 severely injured tissue. Three-Way ANOVA performed to analyze transcriptional levels across gene, region, and
730 injury. ***C***, Gene ontology enrichment and KEGG (Kyoto Encyclopedia of Genes and Genomes) hierarchical
731 clustering for top 10% of upregulated genes in superficial gray matter. ***D***, Gene ontology enrichment and KEGG
732 clustering for top 10% of downregulated genes in superficial gray matter.

733

Figure 4:

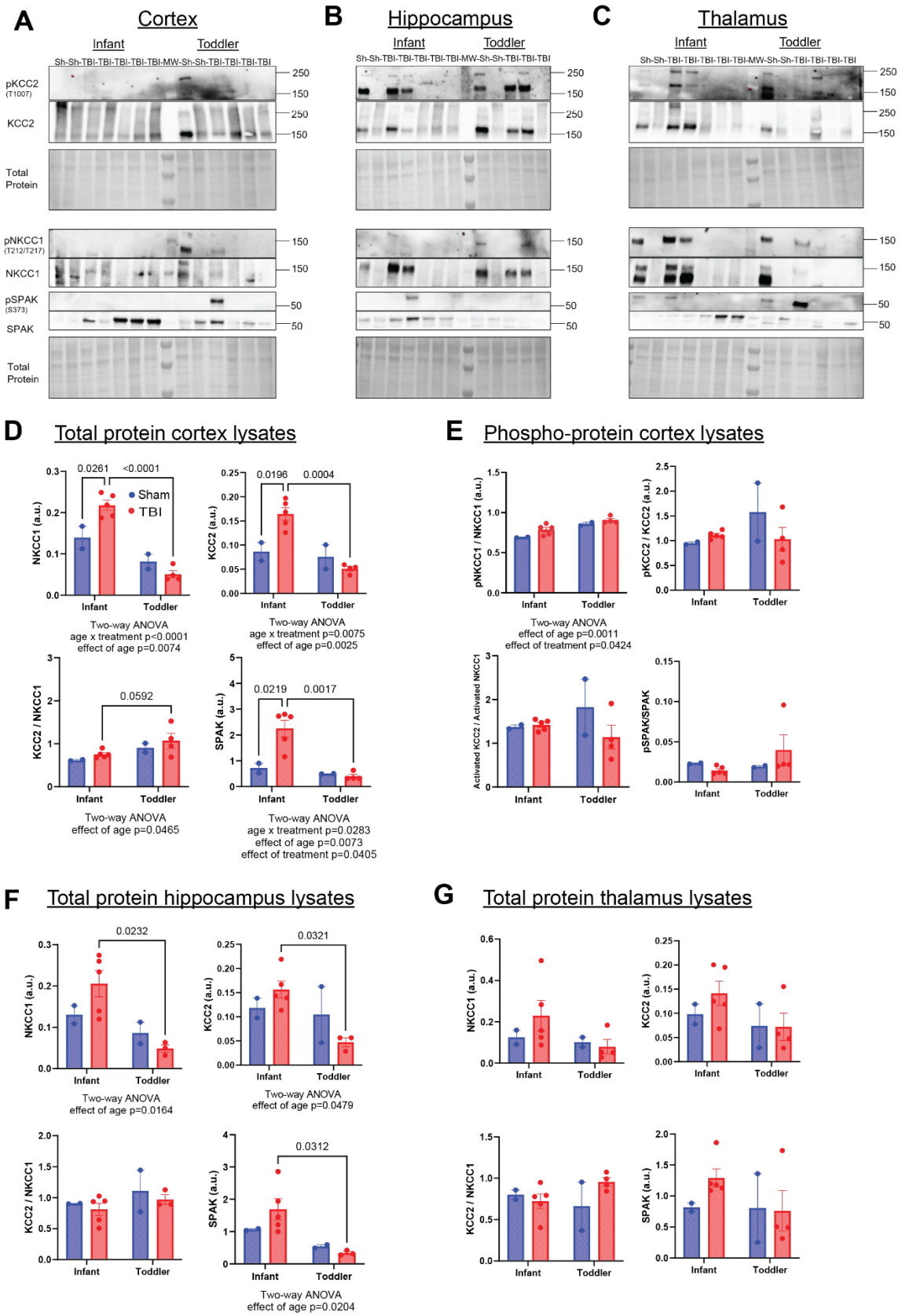
A
Cortex
Infant
Toddler
Sh-Sh-TBI-TBI-TBI-TBI-MW-Sh-Sh-TBI-TBI-TBI-TBI
pKCC2 (T1007)
KCC2
Total Protein
pNKCC1 (T212/T217)
NKCC1
pSPAK (S373)
SPAK
Total Protein
B
Hippocampus
C
Thalamus
D
Total protein cortex lysates
Sham
TBI
NKCC1 (a.u.)
KCC2 (a.u.)
KCC2 / NKCC1
SPAK (a.u.)
Two-way ANOVA
age x treatment p<0.0001
effect of age p=0.0074
Two-way ANOVA
age x treatment p=0.0075
effect of age p=0.0025
Two-way ANOVA
effect of age p=0.0465
Two-way ANOVA
age x treatment p=0.0283
effect of age p=0.0073
effect of treatment p=0.0405
E
Phospho-protein cortex lysates
pNKCC1 / NKCC1 (a.u.)
pKCC2 / KCC2 (a.u.)
Activated KCC2 / Activated NKCC1
pSPAK/SPAK
Two-way ANOVA
effect of age p=0.0011
effect of treatment p=0.0424
F
Total protein hippocampus lysates
Two-way ANOVA
effect of age p=0.0164
Two-way ANOVA
effect of age p=0.0479
Two-way ANOVA
effect of age p=0.0204
G
Total protein thalamus lysates

737 **Figure 4: The cortex and hippocampus were most sensitive to severe TBI injuires with upregulation of**
738 **NKCC1, KCC2, and SPAK abundance and phosphorylation unchanged, and thalamus was unaffected.**
739 Western blots for all biological replicates for infant and toddler piglets receiving sham or severe TBI injuries in
740 cortex (***A***), hippocampus, (***B***), or thalamus (***C***). NKCC1, KCC2, and SPAK increased in cortex of infant piglets,
741 but not toddler piglets with TBI injuries, and the increase of KCC2/NKCC1 is driven by age, not treatment (***D***).
742 Levels of phosphorylated NKCC1 were affected by age and treatment, but not pKCC2, pKCC2/pNKCC1, or
743 pSPAK in cortex (***E***). NKCC1, KCC2, and SPAK increased in hippocampus of infant piglets, but not toddler
744 piglets with TBI injuries, and with no age or treatment effects on KCC2/NKCC1 (***F***). The levels of NKCC1, KCC2,
745 KCC2/NKCC1, and SPAK were unchanged in thalamus across ages and injury (***G***). Two-way ANOVA performed
746 with posthoc multiple t-tests, exact p-values reported on graph.

747

Figure 5:

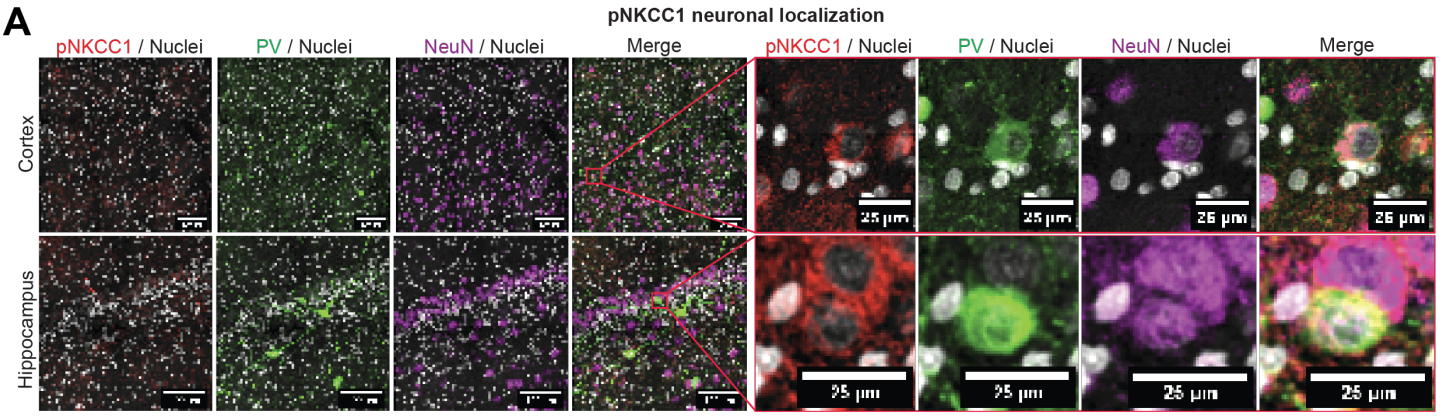

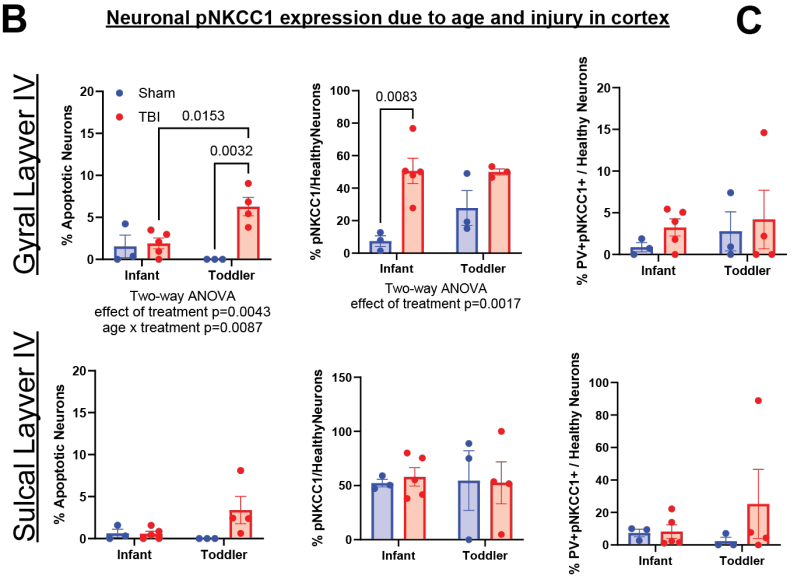

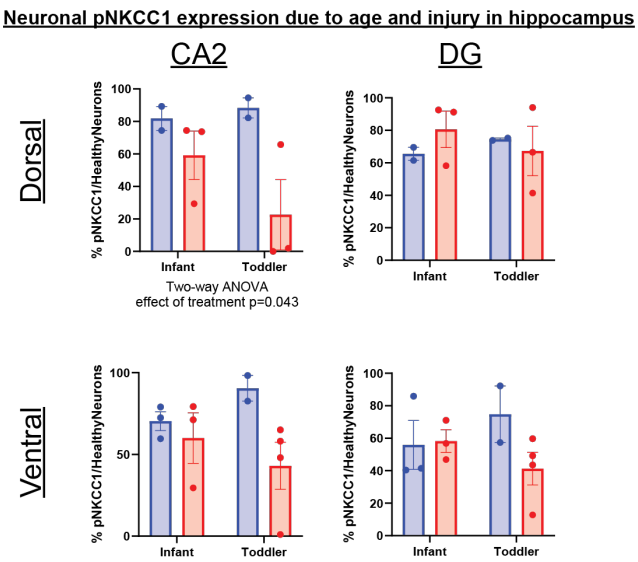

D

		Damage on H&E	SAH %	SDH %	Neuro Score	Total Seizures
Infant	Sham	0.41 ± 0.12 (0.24 - 0.68)	0 ± 0 (0 - 0)	4.85 ± 2.1 (0 - 8.8)	15.5 ± 1.74 (13.25 - 19.25)	0 ± 0 (0 - 0)
	TBI	9.49 ± 3.95 (0.82 - 24.68)	0.46 ± 0.27 (0.03 - 1.81)	25.38 ± 5.81 (14.8 - 47)	13.08 ± 0.92 (10.25 - 15.75)	198 ± 58.2 (30 - 375)
Toddler	Sham	1.91 ± 0.78 (0.29 - 3.62)	0 ± 0 (0 -0.01)	0 ± 0 (0 - 0)	19.75 ± 0.2 (19.25 - 20)	0 ± 0 (0 - 0)
	TBI	23.04 ± 8.82 (2.96 - 50.89)	0.43 ± 0.21 (0.03 - 1.2)	55.1 ± 6.52 (45.5 - 73.5)	11.08 ± 1.42 (7 - 15.5)	157.5 ± 70.45 (0 - 375)

Swine Pediatric Severe TBI Model Characteristics

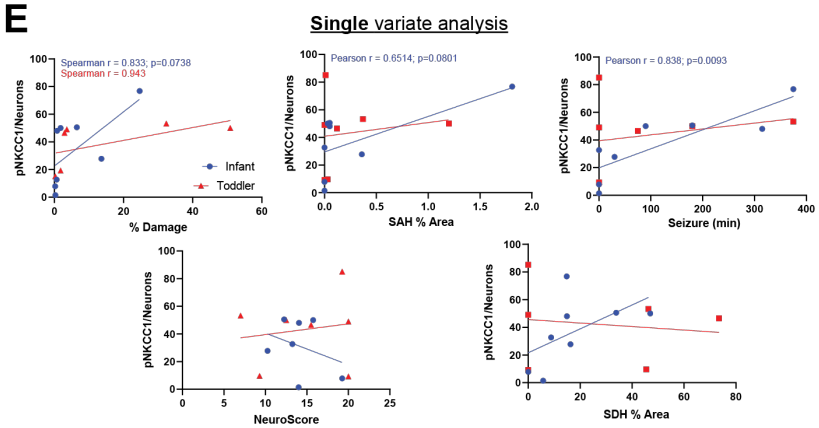

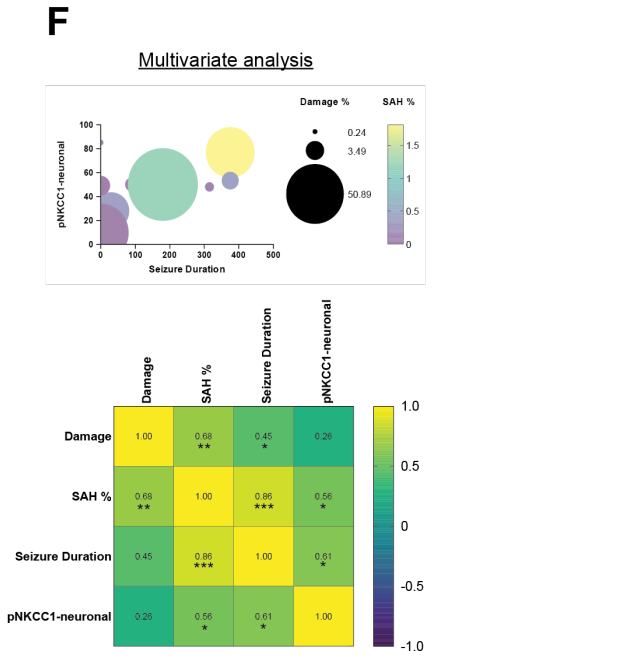

751 **Figure 5: Cortical non-apoptotic, PV$^-$ neurons upregulate pNKCC1 acutely following TBI injuries and**
752 **are associated with burden of tissue damage across ages and burden of subarachnoid hemorrhage**
753 **and seizure duration in infant piglets with TBI.**
754 Immunohistochemical staining for pNKCC1 (red), parvalbumin (green), NeuN (magenta), and nuclei (white), (***A***).
755 (***B***), percentage of apoptotic neurons, % of neuronal pNKCC1 expression, and % PV+ neuronal pNKCC1
756 expression due to age and injury in cortex in gyral or sulcal layer IV populations. Two-way ANOVA performed
757 with posthoc multiple t-tests, exact p-values reported on graph. (***C***), percentage of neuronal pNKCC1 expression
758 in dorsal or ventral CA2 (cornu ammnionis region 2) and DG (dentate gyrus) due to age and injury. Two-way
759 ANOVA performed with posthoc multiple t-tests, exact p-values reported on graph. (***D***), Injury characteristics as
760 unique variables, single variate analysis (***E***) performed across age and correlations (Pearson parametric or
761 Spearman non-parametric) shown on graphs. Multivariate analysis performed and correlation matrices
762 presented (***F***).

763
764

765 **Figure 6:**

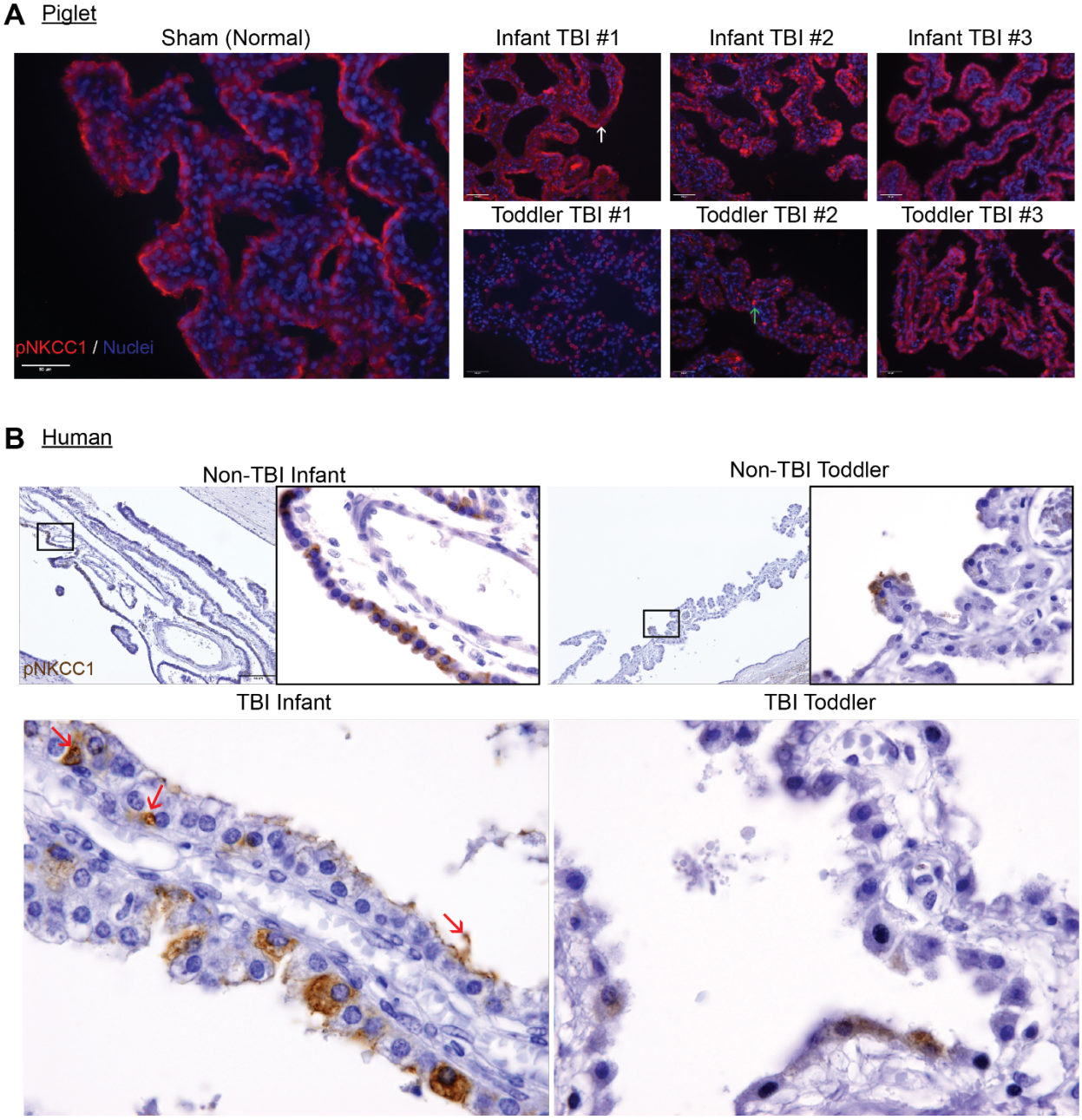

766
767 **Figure 6: pNKCC1 signal becomes irregular in choroid plexus following TBI in piglets and humans.**
768 Representative fluorescent immunohistochemical staining in piglets for choroid plexus pNKCC1 (red) and nuclei
769 (blue) in sham, normal animals compared to infant and toddler pigs with TBI injuries, ***A***. White arrow shows shift
770 from apical to cytosolic localization, green arrows show regions of "fragmented" or "irregular" signal. ***B***,
771 Representative chromogenic immunohistochemical staining of pNKCC1 in choroid plexus in humans with or
772 without TBI. Non-TBI infants and toddlers show pNKCC1 restricted to epithelial cells of ChP, localization is
773 cytosolic and apical, with infants having more pNKCC1 signal than toddlers. In infant TBI, pNKCC1 signal
774 distribution is altered (red arrows). In toddler TBI, pNKCC1 signal is infrequently observed. In TBI, damage to
775 the ChP is apparent, particularly in toddlers.

776

Table 1: Human Sample Demographics

	Sample IDs	PNA (GA)	Sex	Diagnosis	PMI (hr)
Frozen/FFPE Hippocampus (Figure 2)	1	0.4 (40)	Female	Fatty acid oxidation disorder	15
	2	0 (41)	Female	Neonatal bradycardia with arrest and meconium aspiration	12.8
	3	17 (26.5)	Female	Acute asphyxiation	9
	4	12 (32)	Male	Acute asphyxiation	9
	5	5 (40)	Male	Acute asphyxiation	5
	6	11 (36)	Female	Acute asphyxiation	27
	7	13.5 (37.5)	Female	Acute asphyxiation	29
	8	16 (40)	Female	Acute asphyxiation	9
	9	26 (36)	Male	Acute asphyxiation	9
	10	33.4 (38.5)	Male	Intussuseption of inverted Merkel's diverticulum	13
	11	35 (39)	Female	Acute asphyxiation	29
FFPE Non-TBI Control (Figure 6, Supplemental File 1)	Non-TBI-1	0 (23)	Unknown	Normal brain development; labor/pregnancy complications	<24
	Non-TBI-2	0 (27)			
	Non-TBI-3	0 (39)			
	Non-TBI-4	0 (40)			
	Non-TBI-5	4 month	Male	Sudden unexpected death in infancy	24
	Non-TBI-6	5 month	Male	Cystic fibrosis	3.33
	Non-TBI-7	4 year	Female	Acute peritonitis	24
FFPE TBI (Figure 6, Supplemental File 1)	TBI - 1	3 month	Female	Blunt force head injury	23
	TBI - 2	3 year	Female	Traumatic axonal injury, subdural hematoma	24
	TBI - 3	3 year	Male	Road traffic accident, contusions, cerebral edema	24
	TBI - 4	9 year	Female	Road traffic accident, contusions, cerebral edema, subdural hematoma, global ischemia	24
	TBI - 5	9 year	Male	Road traffic accident, contusions, cerebral edema, subdural hematoma, global ischemia	24
	TBI - 6	10 year	Female	Road traffic accident, contusions, cerebral edema	72

780 **Table 2: Antibody information.**

Antibody	Species	Target	Company	Catalog #	Validation Method	WB	IHC
NKCC1	Rabbit	Synthetic Arg77 of mouse NKCC1	Cell Signaling Technology	14581	KO lysate	1:1000	
pNKCC1	Rabbit	Human pNKCC1 Th212/217	Millipore	ABS1004	KO lysate	1:500	1:250
SPAK	Mouse	GST-tagged c-terminus of human STK39	Millipore	MABS178	(+) ctrl human brain tissue	1:1000	
pSPAK	Rabbit	Human pSPAK Ser373	Millipore	07-2273	Hypotonic HEK293 cells	1:500	
KCC2	Rabbit	Synthetic peptide	Abcam	ab259969	(+) and (-) ctrl tissue lysates	1:2000	
pKCC2	Rabbit	Synthetic Ser940	Invitrogen	PA5-95678	KO lysate	1:1000	
Parvalbumin	Sheep	E. coli-derived recombinant human Parvalbumin alpha Ser2-Ser110	Invitrogen	PA5-47693	(+) ctrl brain tissue		1:100
NeuN	Conj 647	Synthetic peptide	Abcam	ab190565	(+) ctrl brain tissue		1:500

781

782 **Table 3: Taqman probe information**

Target	Species	Sequence
Nkcc1	*Human*	*Hs01074325_m1*
Kcc2	*Human*	*Hs00221168_m1*
Stk39	*Mouse*	*Mm01270753_m1*
Reference Gene (18s)	*N/A*	*Hs99999901_s1*

783

Supplemental Figure 1: Transcriptional changes to *Slc12a2*, *Slc12a5*, and *Stk39* due to age and injury in piglets.
Quantitative PCR analysis for transcripts of *Stk39*, *Slc12a5*, and *Slc12a2* due to age, injury, and region in piglets, presented as fold change from sham PND7 piglets. Two-way ANOVA results detailed in table on right and post-hoc multiple t-tests exact p values included on graphs where applicable.

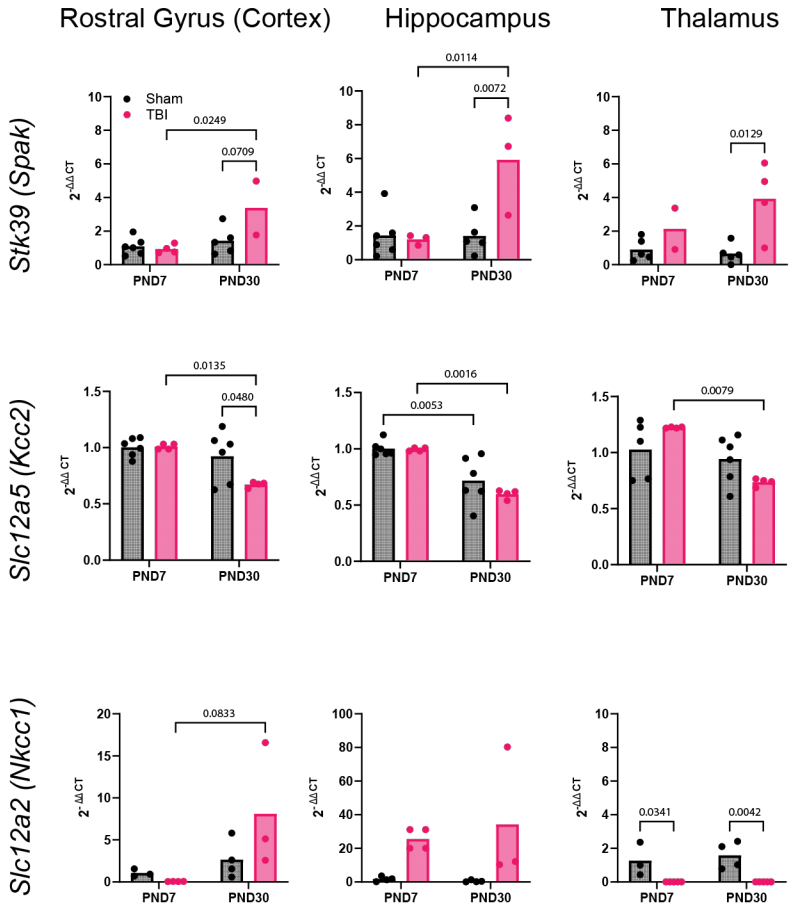

	Rostral Gyrus	Hippocampus	Thalamus
Age	0.0086	0.0104	0.2886
Treatment	0.0688	0.0176	0.0073
Age x Treatment	0.0352	0.0097	0.1703

	Rostral Gyrus	Hippocampus	Thalamus
Age	0.0039	0.00001	0.0038
Treatment	0.0636	0.2677	0.9538
Age x Treatment	0.0535	0.3256	0.0293

	Rostral Gyrus	Hippocampus	Thalamus
Age	0.0314	0.6891	0.5661
Treatment	0.2754	0.0085	0.0002
Age x Treatment	0.124	0.5932	0.5661

Supplemental Figure 2:
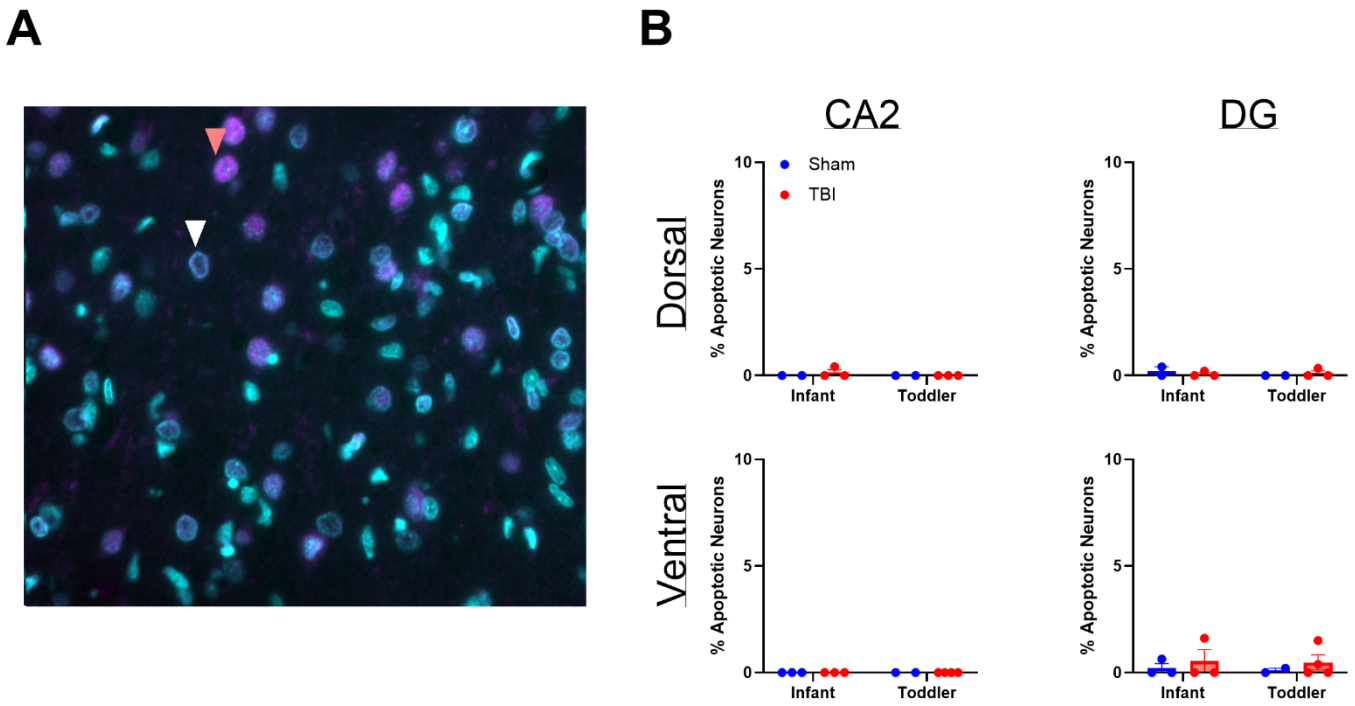
Examples of healthy neurons (peach arrowhead) and dead neurons (white arrowhead) in cortex as assessed by nuclear stain (cyan) and NeuN^{+} (magenta), ***A***. Counts for apoptotic neurons in dorsal or ventral CA2 and DG regions in hippocampus due to age and injury, ***B***.